Respiratory Alkalosis Provokes Spike-Wave Discharges in Seizure-Prone Rats

Author names and affiliations

Kathryn A. Salvati[1,2*], George M.P.R. Souza[1], Adam C. Lu[1,2], Matthew L. Ritger[1,2], Patrice G. Guyenet[1], Stephen B. Abbott[1], Mark P. Beenhakker[1*]

[1] Department of Pharmacology, University of Virginia, Charlottesville, VA, USA.

[2] Neuroscience Graduate Program, University of Virginia, Charlottesville, VA, USA.

[*]Co-corresponding authors

25 **Abstract**

26 Hyperventilation reliably provokes seizures in patients diagnosed with absence epilepsy.
27 Despite this predictable patient response, the mechanisms that enable hyperventilation to
28 powerfully activate absence seizure-generating circuits remain entirely unknown. By utilizing
29 gas exchange manipulations and optogenetics in the WAG/Rij rat, an established rodent model
30 of absence epilepsy, we demonstrate that absence seizures are highly sensitive to arterial
31 carbon dioxide, suggesting that seizure-generating circuits are sensitive to pH. Moreover,
32 hyperventilation consistently activated neurons within the intralaminar nuclei of the thalamus, a
33 structure implicated in seizure generation. We show that intralaminar thalamus also contains
34 pH-sensitive neurons. Collectively, these observations suggest that hyperventilation activates
35 pH-sensitive neurons of the intralaminar nuclei to provoke absence seizures.

36

37 **Introduction**

38 Epilepsy is a common neurological disorder characterized by recurrent and spontaneous
39 seizures. Yet, accumulating evidence indicates that seizures are not necessarily unpredictable
40 events (Amengual-Gual et al., 2019; Bartolini & Sander, 2019; Baud et al., 2018; Ferlisi &
41 Shorvon, 2014). Several factors affect seizure occurrence, including metabolism (Lusardi et al.,
42 2015; Masino et al., 2012; Masino & Rho, 2012, 2019), sleep (Bazil, 2019; Fountain et al., 1998;
43 Malow et al., 1999; Nobili et al., 2001), catamenia (Herzog & Frye, 2014; Joshi & Kapur, 2019;
44 Reddy et al., 2001), light (Padmanaban et al., 2019) and circadian rhythm (Amengual-Gual et
45 al., 2019; Debski et al., 2020; Smyk & van Luijtelaar, 2020; Stirling et al., 2021). In extreme
46 cases, stimuli immediately provoke seizures, a condition known as *reflex epilepsy* (Kasteleijn-
47 Nolst Trenité, 2012; Koepp et al., 2016). The mechanisms that render certain seizure-
48 generating networks susceptible to external factors remain unknown.

49 A highly reliable seizure trigger associated with childhood absence epilepsy is
50 hyperventilation. Between 87-100% of all children diagnosed with the common *Genetic*

51 *Generalized Epilepsy* produce spike-wave seizures upon voluntary hyperventilation (Hughes, 52 2009; Ma et al., 2011; Sadleir et al., 2009). Indeed, hyperventilation serves as a powerful tool 53 for diagnosing this childhood epilepsy (Adams & Lueders, 1981; Holowach et al., 1962; Sadleir 54 et al., 2006; Watemberg et al., 2015). Remarkably, as no single genetic etiology drives absence 55 epilepsy (Chen et al., 2013; Crunelli & Leresche, 2002; Helbig, 2015; Koeleman, 2018; 56 Robinson et al., 2002; Xie et al., 2019), hyperventilation appears to recruit fundamental seizure- 57 generating mechanisms shared by virtually all patients.

58 Exhalation of CO_2 during hyperventilation causes hypocapnia, a state of decreased 59 arterial CO_2 partial pressure ($PaCO_2$), and respiratory alkalosis, a state of elevated arterial pH 60 (Laffey & Kavanagh, 2002). Hyperventilation also causes rapid arterial vasoconstriction (Raichle 61 & Plum, 1972) and increased cardiac output (Donevan et al., 1962). Recent work demonstrates 62 that inspiration of 5% CO_2 blunts hyperventilation-provoked spike-wave seizures in humans 63 (Yang et al., 2014). Collectively, these observations suggest that respiratory alkalosis serves as 64 the primary trigger for hyperventilation-provoked absence seizures.

65 Spike-wave seizures associated with absence epilepsy arise from hypersynchronous 66 neural activity patterns within interconnected circuits between the thalamus and the cortex 67 (Avoli, 2012; Beenhakker & Huguenard, 2009; Huguenard & McCormick, 2007; McCafferty et 68 al., 2018; McCormick & Contreras, 2001; Meeren et al., 2002). The crux of the prevailing model 69 describing absence seizure generation includes an initiating bout of synchronous activity within 70 the somatosensory cortex that recruits rhythmically active circuits in the thalamus (Meeren et 71 al., 2002; Sarrigiannis et al., 2018). With widespread connectivity to the cortex, the thalamus 72 then rapidly generalizes spike-wave seizures to other brain structures. The extent to which 73 thalamocortical circuits respond to shifts in pH during hyperventilation-induced respiratory 74 alkalosis is unknown.

75 Herein, we test the hypothesis that respiratory alkalosis regulates the occurrence of 76 spike-wave seizures. We demonstrate that hyperventilation-provoked absence seizures

77 observed in humans can be mimicked in an established rodent model, the WAG/Rij rat
78 (Coenen, 2003; Coenen et al., 1992; Russo et al., 2016; van Luijtelaar & Coenen, 1986). We
79 first show that hyperventilation induced with hypoxia reliably evokes respiratory alkalosis and
80 increases spike-wave seizure count in the WAG/Rij rat. When supplemented with 5% CO_2 to
81 offset respiratory alkalosis, hypoxia did not increase spike-wave seizure count. Moreover,
82 hypercapnia alone (high $PaCO_2$) reduced spike-wave seizure count despite a robust increase in
83 respiration rate. We also show that optogenetic stimulation of brainstem respiratory centers to
84 produce respiratory alkalosis during normoxia induces CO_2-sensitive spike-wave seizures.
85 Collectively, these results identify respiratory alkalosis as the primary seizure trigger in absence
86 epilepsy following hyperventilation. Finally, we show that structures of the intralaminar thalamic
87 nuclei are both (1) activated during respiratory alkalosis, and (2) pH-sensitive. Thus, our data
88 demonstrate that respiratory alkalosis provokes spike-wave seizures and shine a spotlight on
89 the poorly understood intralaminar thalamus in the pathophysiology of spike-wave seizures.
90

91 **Results**

92 *Hypoxia triggers spike-wave seizures in the WAG/Rij rat*

93 We first set out to determine if an accepted rat model of absence epilepsy, the WAG/Rij
94 rat, recapitulates hyperventilation-provoked absence seizures, as observed in humans. We
95 combined whole-body plethysmography and electrocorticography/electromyography
96 (ECoG/EMG) recordings in awake WAG/Rij rats to assess respiration and spike-wave seizure
97 occurrence while exposing animals to different gas mixtures of O_2, CO_2 and N_2 (Figure 1A,B).
98 We only considered spike-wave seizures that persisted for a minimum of two seconds and
99 occurred concomitantly with behavioral arrest in the animal. Spike-wave seizures are
100 distinguishable from non-REM sleep based on the appearance of 5-8 Hz frequency harmonics
101 in the power spectrogram (see Figure 1B, *expanded trace*).

102 We first compared respiration and ECoG/EMG activity in rats exposed to atmospheric
103 conditions (i.e., normoxia: <u>21%</u> O_2; <u>0%</u> CO_2; <u>79%</u> N_2) and hypoxia (<u>10%</u> O_2; <u>0%</u> CO_2; <u>90%</u> N_2).
104 Hypoxia reliably stimulates rapid breathing, blood alkalosis and hypocapnia in rats (Basting et
105 al., 2015; Souza et al., 2019). We cycled rats between 40-minute epochs of normoxia and 20-
106 minute epochs of hypoxia. O_2 levels were measured from the outflow of the plethysmography
107 chamber for confirmation of gas exchange (Figure 1B, *top*). Hypoxia evoked a robust increase
108 in respiratory rate (Figure 1B, *expanded*) and reliably provoked seizures. A peristimulus time
109 histogram (PSTH) aligned to the onset of gas exchange shows spike-wave seizure counts
110 during the 15 minutes immediately before and during hypoxia (Figure 1C1); the PSTH shows
111 the contribution of each rat in stacked histogram format. Respiratory rates confirmed that
112 hypoxia increased ventilation (Figure 1C2,3). To quantify the effect of hypoxia on seizures, we
113 calculated the mean spike-wave seizure count across all bins for each rat. Relative to normoxia,
114 spike-wave seizure count during hypoxia was nearly 2-fold higher ($p = 4.5 \times 10^{-7}$, $n = 15$; Fig.
115 1D) and respiratory rate increased by 30% ($p = 1.6 \times 10^{-5}$, $n = 15$; Fig. 1E). Whereas the
116 duration of individual spike-wave seizures was not altered by hypoxia (normoxia: 5.3 ± 0.4 sec;
117 hypoxia: 5.8 ± 0.4 sec; $p = 0.56$, $n = 15$), the frequency of individual events was lower
118 (normoxia: 7.6 ± 0.12 Hz; hypoxia: 5.8 ± 0.4 Hz; $p = 4.7 \times 10^{-5}$, $n = 15$).

119 Recent work shows that spike-wave seizures commonly occur in several rat strains,
120 including those that are generally not considered epileptic (Taylor et al., 2017, 2019). While
121 between 62% (Vergnes et al., 1982) and 84% (Robinson & Gilmore, 1980) of Wistar rats do not
122 have seizures, we nonetheless tested whether hypoxia can unmask seizure-generating potential
123 in this strain, as Wistar and WAG/Rij rats share the same genetic background (Festing, 1979).
124 In normoxia, seizures were absent in all four Wistar rats we tested, consistent with the
125 infrequent spike-wave seizure occurrence reported for this strain. Relative to normoxia in Wistar
126 rats, hypoxia induced hyperventilation, hypocapnia and blood alkalization but did not provoke
127 spike-wave seizures (Figure 2; see Table 5). Instead, hypoxia primarily triggered arousal in

128 Wistar rats, as revealed in EEG spectrograms by the reduction in sleep-related frequencies.
129 Therefore, we hypothesize that hypoxia-provoked spike-wave seizures are unique to seizure-
130 prone rodent models, just as hyperventilation does not provoke absence seizures in otherwise
131 healthy humans.
132

133 *CO_2 suppresses spike-wave seizures*

134 Hyperventilation promotes hypocapnia, a state of low $PaCO_2$. As dissolved CO_2 is acidic,
135 hyperventilation-triggered hypocapnia is also associated with respiratory alkalosis. To test the
136 hypothesis that hypocapnia specifically provokes seizures, we next determined whether
137 supplemental CO_2 (5%) blunts the spike-wave seizure-provoking effects of hypoxia. We
138 performed ECoG/plethysmography experiments as before but alternated between two test trials:
139 hypoxia and hypoxia/hypercapnia (10% O_2, 5% CO_2; 85% N_2). Test trials were interleaved with
140 40-minute periods of normoxia to allow blood gases to return to baseline levels (Figure 3A). As
141 before, hypoxia increased spike-wave seizure count by nearly 2-fold ($p = 1.76 \times 10^{-6}$, n = 9;
142 Figure 3B1, C) and increased respiratory rate by 27% ($p = 6.59 \times 10^{-4}$, n = 9; Figure 3B3, D).
143 Also as before, the duration of individual spike-wave seizures was not altered by hypoxia
144 (normoxia: 5.5 ± 0.5 sec; hypoxia: 6.3 ± 0.5 sec; p = 0.26, n = 9), but the frequency of individual
145 events was lower (normoxia: 7.7 ± 0.2 Hz; hypoxia: 6.3 ± 0.5 Hz; p = 0.014, n = 9). In the same
146 rats, supplementing hypoxia with 5% CO_2 suppressed the spike-wave seizure response insofar
147 that hypoxia/hypercapnia did not change spike-wave seizure count relative to normoxia (p =
148 0.18, n = 9; Figures 3E1 and 3F) despite a predictable and robust elevation in respiratory rate (p
149 $= 2.71 \times 10^{-4}$, n = 9; Figures 3E2, 3 and 3G). Relative to normoxia, the duration of individual
150 spike-wave seizures was elevated during hypoxia/hypercapnia (normoxia: 5.5 ± 0.6 sec;
151 hypoxia/hypercapnia: 7.5 ± 1.0 sec; p = 0.006, n = 9), but the frequency of individual spike-wave
152 seizures was unchanged (normoxia: 7.8 ± 0.1 Hz; hypoxia/hypercapnia: 7.5 ± 1.0 Hz; p = 0.77,
153 n = 9).

154 In a separate cohort of rats, we collected arterial blood samples to measure blood
155 $PaCO_2$, PaO_2 and pH during normoxia, hypoxia and hypoxia/hypercapnia (see Table 6). We
156 observed a considerable change in PaO_2 [F (1.056, 5.281) = 406.4, p = 3.0 x 10^{-6}], $PaCO_2$ [F
157 (1.641, 8.203) = 338.9, p = 1.9 x 10^{-8}] and pH [F (1.938, 9.688) = 606, p = 7.2 x 10^{-11}] values
158 among the three conditions. Hypoxia decreased $PaCO_2$ (p = 2.1 x 10^{-6}; n = 6; Figure 3H2) and
159 concomitantly alkalized the blood (p = 7.0 x 10^{-6}, n = 6; Figure 3H3). We also observed a
160 decrease in PaO_2 (p =
161 6.0 x 10^{-6}; n = 6; Figure 3H1). Supplemental CO_2 returned blood pH (p = 0.008, n = 6; Figure
162 3H3)
163 and PaCO2 (p = 0.42, n = 6; Figure 3H2) to normoxia levels. However, heightened respiratory
164 rate in supplemental CO_2 raised PaO_2 (p = 00013, n = 6; Figure 3H1). Collectively, these data
165 support the hypothesis that blood pH powerfully regulates spike-wave seizure activity.
166 Next, we tested whether supplementing normoxia with 5% CO_2 is sufficient to reduce
167 spike-wave seizure counts. Respiration during high CO_2 causes hypercapnia, a condition that
168 increases blood $PaCO_2$ and acidifies the blood (Eldridge et al., 1984). As with hypoxia,
169 hypercapnia also triggers hyperventilation (Guyenet et al., 2019). We performed
170 ECoG/plethysmography experiments in rats that cycled through trials of normoxia and
171 hypercapnia (21% O_2; 5% CO_2; 74% N_2) and compared the mean number of seizures observed
172 during the two conditions. Relative to normoxia, the number of spike-wave seizures was lower
173 during 5% CO_2 (p = 0.0028, n = 8; Figure 4B1 and 4C); hypercapnia also induced a powerful
174 respiratory response (p = 3.78 x 10^{-5}, n = 8; Figure 4B2,3 and 4D). Hypercapnia neither
175 changed the duration (normoxia: 5.6 ± 0.4 sec; hypercapnia: 6.2 ± 0.4 sec; p = 0.22, n = 8) nor
176 the frequency (normoxia: 6.1 ± 1.0 Hz; hypercapnia: 6.2 ± 0.4 Hz; p = 0.28, n = 8) of individual
177 spike-wave seizures. Blood gas measurements revealed that 5% hypercapnia increased $PaCO_2$
178 (p = 0.022, n = 6; Figure 4E2) and slightly acidified blood pH (p = 0.00063, n = 6; Figure 4E3).
179 These results provide further support for the hypothesis that the neural circuits that produce

180 spike-wave seizures are CO_2-sensitive, and thus pH-sensitive. Moreover, the results
181 demonstrate that neither the mechanics of elevated ventilation, nor increased arousal, is
182 sufficient to provoke spike-wave seizures.
183
184 *Optogenetic stimulation of the retrotrapezoid nucleus provokes spike-wave seizures*
185 In addition to inducing hyperventilation and hypocapnia, hypoxia also lowers PaO_2 (see
186 Figure 3H1), an effect that stimulates the carotid body, the principal peripheral chemoreceptor
187 that initiates hyperventilation during hypoxic conditions (Lindsey et al., 2018; López-Barneo et
188 al., 2016; Semenza & Prabhakar, 2018). Carotid body activity recruits neurons of the nucleus
189 tractus solitarius (NTS) that then excite neurons of the central respiratory pattern generator to
190 drive a respiratory response (Guyenet, 2014; López-Barneo et al., 2016). To evaluate the
191 capacity of hyperventilation to provoke seizures in the absence of hypoxia (and, therefore, in the
192 absence of
193 carotid body activation), we utilized an alternative approach to induce hyperventilation. Under
194 physiological conditions, chemosensitive neurons of the retrotrapezoid nucleus (RTN), a
195 brainstem respiratory center, are activated during an increase in $PaCO_2$ and a consequent drop
196 in arterial pH (Guyenet et al., 2016, 2019; Guyenet & Bayliss, 2015) that then stimulate
197 respiration. Optogenetic activation of RTN neurons in normoxia is sufficient to evoke a powerful
198 hyperventilatory response that alkalizes the blood (Abbott et al., 2011; Souza et al., 2020).
199 Importantly, PaO_2 remains stable (or is slightly elevated) during optogenetically-induced
200 respiration. Therefore, hyperventilation evoked by optogenetic RTN activation during normoxia
201 both (1) promotes respiratory alkalosis without hypoxia and (2) is a more clinically relevant
202 approximation of voluntary hyperventilation than hypoxia-induced hyperventilation.
203 We selectively transduced RTN neurons of WAG/Rij rats with a lentiviral approach using
204 the PRSX8 promoter to drive channelrhodopsin expression (Abbott et al., 2009; Hwang et al.,
205 2001; Lonergan et al., 2005; Figure 5A, B). Once channelrhodopsin was expressed, we

206 challenged rats with two test trials: RTN photostimulation during normoxia and RTN
207 photostimulation during hypercapnia (Figure 5C); in a subset of animals, we cycled rats
208 between the two conditions. In both trials, laser stimulation was delivered with trains of stimuli.
209 During each train, the laser was pulsed at 20 Hz (10msec pulse) for two seconds. The laser was
210 then off for 2 seconds (i.e., intertrain interval = two seconds, see Figure 5C). This train stimulus
211 was repeated for 15 minutes. Laser stimulation during normoxia provoked spike-wave seizures
212 ($p = 0.002$; $n = 10$; Figures 5D, 5E1 and 5F) and also increased ventilation ($p = 0.019$; $n = 10$;
213 Figures 5E2,3 and 5G). Laser stimulation during normoxia did not alter the duration of individual
214 spike-wave seizures (normoxia: 4.3 ± 0.6 sec; normoxia-laser: 4.6 ± 0.5 sec; $p = 0.51$, $n = 10$).
215 By contrast, the frequency of individual spike-wave seizures was lower during laser stimulation,
216 relative to normoxia-alone (normoxia: 7.5 ± 0.2 Hz; normoxia-laser: 4.6 ± 0.5 Hz; $p = 2.2 \times 10^{-4}$,
217 $n = 10$). Laser stimulation during hypercapnia in the same animals did not alter spike-wave
218 seizure count ($p = 0.86$; $n = 6$; Figures 5H1 and 5I), despite the induction of a strong
219 hyperventilatory response ($p = 0.031$; $n = 6$; Figures 5H2,3 and 5J). We observed no difference
220 in duration (normoxia: 6.8 ± 1.0 sec; hypercapnia-laser: 6.9 ± 1.0 sec; $p = 0.88$, $n = 6$) or
221 frequency (normoxia: 7.9 ± 0.2 Hz; hypercapnia-laser: 6.9 ± 1.0 Hz; $p = 0.33$, $n = 6$) of individual
222 spike-wave seizures during normoxia versus hypercapnia coupled with laser stimulation. In
223 sum, these results support the hypothesis that respiratory alkalosis is necessary to provoke
224 seizures during hyperventilation and excludes carotid body activation as a contributing factor.
225
226 *Hypoxia-induced hyperventilation activates neurons of the intralaminar thalamus*
227 Thus far, our results demonstrated that respiratory alkalosis (i.e., hyperventilation that promotes
228 a net decrease in $PaCO_2$) provokes spike-wave seizures in the WAG/Rij rat. Next, we sought to
229 identify brain structures activated during respiratory alkalosis that may contribute to spike-wave
230 seizure provocation. We used the neuronal activity marker cFos to identify such structures in
231 WAG/Rij rats. To isolate activation specifically associated with respiratory alkalosis, we first

232 administered ethosuximide (200mg/kg, i.p.) to suppress spike-wave seizures; respiration and
233 ECoG/EMG signals confirmed ventilatory responses and spike-wave seizure suppression.
234 Ethosuximide-injected rats were exposed to either hypoxia, normoxia or hypoxia/hypercapnia
235 for 30 minutes and then transcardially perfused 90 minutes later. Brains were harvested and
236 evaluated for cFos immunoreactivity. Surprisingly, in rats exposed to hypoxia we observed
237 heightened immunoreactivity in the intralaminar nuclei, a group of higher-order thalamic nuclei
238 that, unlike first-order thalamic nuclei, do not receive peripheral sensory information (Saalmann,
239 2014) (Figure 6A,B). Indeed, cFos immunoreactivity was largely absent from first-order thalamic
240 nuclei and cortex, and was blunted in rats treated with normoxia and hypoxia/hypercapnia
241 (Figure 6B). Importantly, the latter condition elevates respiration but normalizes arterial pH (see
242 Figure 3G and 3H). Immunoreactivity quantification revealed that the number of cFos-positive
243 cells within the intralaminar thalamic nuclei was highest following hypoxia [ANOVA: $F(2, 6) =$
244 31.59, $p = 0.00019$, Figure 6C].

245 As heightened cFos immunoreactivity was observed primarily following hypoxia that
246 results in pronounced respiratory alkalosis, we next tested the hypothesis that neurons of the
247 intralaminar nuclei are pH-sensitive. We stereotaxically delivered the pan-neuronal expressing
248 GCaMP7s (pGP-AAV-syn-jGCaMP7s-WPRE) to the intralaminar nuclei and harvested acute
249 brain sections three weeks later (Figure 6D). Recording fluorescence changes in brain sections
250 revealed that extracellular alkalosis quickly and reversibly activated neurons of the intralaminar
251 nuclei (Figure 6D). An electrophysiological evaluation of pH sensitivity using voltage-clamp
252 recordings (V_{hold} = -50mV) showed that alkaline bathing solutions evoke inward currents in
253 intralaminar neurons (e.g., Figure 6F, G), suggesting that excitatory ion channels and/or
254 receptors were activated. Interestingly, alkaline-induced inward currents appeared blunted in
255 other structures implicated in spike-wave seizure generation, such as somatosensory thalamus
256 and cortex (Figure 6H). These results are consistent with previous reports of blunted,
257 macroscopic pH sensitivity in the somatosensory thalamus (Meuth et al., 2006). Collectively,

258 these results support the hypothesis that respiratory alkalosis activates pH-sensitive neurons of
259 the intralaminar thalamic nuclei in the WAG/Rij rat.
260
261 **Discussion**

262 Hyperventilation-provoked seizures associated with absence epilepsy were first formally
263 described in 1928 by William Lennox (Lennox, 1928) and despite the clinical ubiquity of utilizing
264 hyperventilation to diagnose the common form of childhood epilepsy, no animal studies have
265 attempted to resolve the physiological events that enable hyperventilation to reliably provoke
266 spike-wave seizures. To resolve events and relevant brain structures recruited during this
267 phenomenon, we first utilized the WAG/Rij rat to establish a rodent model that mimics
268 hyperventilation-provoked spike-wave seizures in humans. With this model, we show that
269 hyperventilation only provokes spike-wave seizures in seizure-prone, not generally seizure-free,
270 rats. We then show that supplemental CO_2, by mitigating respiratory alkalosis, suppresses
271 spike-wave seizures triggered by hyperventilation during either hypoxia or direct activation of
272 brainstem respiratory centers. Moreover, supplemental CO_2, by producing respiratory acidosis,
273 suppresses spontaneous spike-wave seizures (i.e., those occurring during normoxia) despite a
274 compensatory
275 increase in respiratory rate. These data demonstrate that spike-wave seizures are yoked to
276 arterial CO_2/pH. Finally, we demonstrate that respiratory alkalosis activates neurons of the
277 intralaminar thalamic nuclei, also in a CO_2-dependent manner; activation of these neurons is
278 also pH-sensitive. With these observations, we propose a working model wherein respiratory
279 alkalosis
280 activates pH-sensitive neurons of the intralaminar nuclei that in turn engage seizure-generating
281 neural circuits to produce spike-wave seizures (Figure 7).
282
283 *Cortical EEG Patterns Evoked by Hyperventilation*

284 Hyperventilation produces stereotypical EEG patterns in both healthy children and
285 children with absence epilepsy (Barker et al., 2012). In healthy children, hyperventilation can
286 evoke an EEG pattern known as *Hyperventilation-Induced, High-Amplitude Rhythmic Slowing*
287 (HIHARS) that is often associated with altered awareness (Barker et al., 2012; Lum et al.,
288 2002). Electrographically, HIHARS is distinct from spike-wave seizures insofar the EEG lacks
289 epilepsy-associated spikes and resembles slow-wave sleep. Nonetheless, age-dependence and
290 behavioral similarities between HIHARS and absence seizures exist (Lum et al., 2002; Mattozzi
291 et al., 2021), thereby supporting the hypothesis that HIHARS and spike-wave seizures borrow
292 from overlapping neural circuit mechanisms (Mattozzi et al., 2021). Indeed, while HIHARS and
293 spike-wave seizures are clearly distinct EEG patterns, human spike-wave seizures observed
294 during hyperventilation are subtly different from those occurring spontaneously (Sadleir et al.,
295 2008), perhaps a reflection of the contribution of EEG-slowing circuitry to spike-wave seizures;
296 while largely similar, we also found some differences in WAG/Rij spike-wave seizure frequency
297 during some manipulations.

298 When viewed alongside work performed in the 1960s by Ira Sherwin (Sherwin, 1965,
299 1967), our results support the hypothesis that hyperventilation-provoked spike-wave seizures
300 and HIHARs share common circuits. Sherwin demonstrated that hyperventilation evokes
301 HIHARS in cats (Sherwin, 1965), and that the stereotyped EEG pattern requires an intact
302 central lateral nucleus of the thalamus (Sherwin, 1967). Together with the central medial (CM)
303 and paracentral thalamic nuclei, the central lateral nucleus belongs to the anterior group of the
304 intralaminar nuclei (Saalmann, 2014), the location of cFos immunoreactivity associated with
305 respiratory alkalosis and pH-sensitivity (Figure 6). Indeed, at the time Sherwin postulated that
306 the intralaminar nuclei of the thalamus are both chemoreceptive and capable of engaging
307 widespread cortical activity (Sherwin, 1967). We now postulate that these nuclei are also
308 instrumental for provoking spike-wave seizures during hyperventilation.

309

310 *Thalamocortical circuit involvement in spike-wave seizures*

311 Decades of work have culminated in a canonical model wherein interconnected
312 circuits between the cortex and thalamus support the initiation and maintenance of generalized
313 spike-wave seizures (Avoli, 2012; Beenhakker & Huguenard, 2009; Huguenard & McCormick,
314 2007; McCafferty et al., 2018; McCormick & Contreras, 2001; Meeren et al., 2002). By recording
315 from multiple sites in the WAG/Rij rat, Meeren et al. (Meeren et al., 2002) concluded that the
316 peri-oral region of somatosensory cortex provides the bout of hypersynchronous activity that
317 initiates a spike-wave seizure. This activity then rapidly recruits additional somatosensory
318 cortices and the

319 lateral dorsal thalamus, a higher-order thalamic nucleus involved in spatial learning and memory
320 (Bezdudnaya & Keller, 2008). Finally, first-order thalamic nuclei that encode somatosensory
321 information (i.e., the ventrobasal complex) are recruited. This stereotyped succession of events
322 occurs within the first 500 milliseconds of the spike-wave seizure, after which the temporal
323 relationships among cortical and thalamic structures are more unpredictable (Meeren et al.,
324 2002). Additional studies support the hypothesis that cortical hyperactivity initiates spike-wave
325 seizures (Pinault, 2003; Pinault et al., 1998) and have motivated what is generally referred to as
326 the *cortical focus theory* for spike-wave seizure initiation (Meeren et al., 2005).

327 While resolving how seizures initiate and propagate through brain structures is of critical
328 importance, such an understanding does not necessarily address the mechanisms that drive the
329 highly rhythmic and hypersynchronous activity associated with ongoing spike-wave seizures.
330 Extensive work on acute brain slice preparations clearly demonstrates that circuits between
331 first-order thalamic nuclei and the reticular thalamic nucleus are sufficient to sustain rhythmic
332 network activities, including those comparable to absence seizures (Bal et al., 1995; Bal &
333 McCormick, 1993; McCormick & Contreras, 2001; von Krosigk et al., 1993). In this model,
334 feedforward inhibition provided by reticular neurons evokes robust, hypersynchronous post-
335 inhibitory rebound bursts among thalamocortical neurons that then relay activity back to reticular

336 thalamus and to cortex. Reticular neuron-mediated feedforward inhibition of thalamocortical
337 neurons, coupled with reciprocal excitation from thalamocortical neurons to reticular neurons,
338 forms the basis of a rhythmogenic circuit that is proposed to maintain spike-wave seizures.
339 While this model very likely accounts for rhythmicity in the acute brain slice preparation, it is
340 becoming less clear how first-order thalamocortical neurons actively contribute to the
341 maintenance of spike-wave seizures recorded *in vivo* (Huguenard, 2019; McCafferty et al.,
342 2018). Moreover, most current models of spike-wave initiation and maintenance neglect the
343 potential contribution of the intralaminar nuclei to seizure initiation and maintenance despite
344 several observations to the contrary.

345 In an effort to resolve structures capable of evoking spike-wave seizures, Jasper and
346 colleagues electrically stimulated several thalamic nuclei in cats while recording EEG. By doing
347 so in both lightly anesthetized (Jasper & Droogleever-Fortuyn, 1947) and unanesthetized
348 (Hunter & Jasper, 1949) animals, the authors concluded that stimulation of the anterior
349 intralaminar nuclei (i.e., central lateral, central medial and paracentral nuclei) was sufficient to
350 evoke spike-wave seizures that outlasted the stimulus; stimulation also produced behavioral
351 repertoires associated with absence seizures. However, stimulation of first-order thalamic nuclei
352 did not evoke spike-wave seizures, nor did it evoke seizure-like behaviors. Consistent with
353 these observations, lesions to the intralaminar nuclei abolish pharmacologically-induced spike-
354 wave seizures in Sprague-Dawley rats (Banerjee & Snead, 1994); seizures persist following
355 lesions to first-order nuclei. More recently, an EEG-fMRI study in human patients also implicates
356 the intralaminar nuclei in the initiation of spontaneous spike-wave seizures (Tyvaert et al.,
357 2009). Regrettably, Meeren et al. (Meeren et al., 2002) did not include intralaminar thalamic
358 recordings during their study of spike-wave seizure propagation in the WAG/Rij rat.
359 Nonetheless, proposing the hypothesis that the intralaminar nuclei, not cortical structures,
360 initiate spike-wave seizures, including those occurring

361 spontaneously (i.e., not during hyperventilation), seems premature. Indeed, the possibility that
362 activation of cortically projecting intralaminar neurons during hyperventilation recruits cortical
363 structures to, in turn, initiate spike-wave seizures is equally plausible. In this model, respiratory
364 alkalosis activates intralaminar neurons that, in turn, directly recruit spike-wave seizure initiation
365 sites in the cortex. Alternatively, activated intralaminar neurons may increase the excitability of
366 the reticular thalamic nucleus, a highly interconnected thalamic hub (Swanson et al., 2019),
367 thereby lowering the threshold required for cortical input to spark a spike-wave seizure (see
368 Figure 7). In support of this latter model, Purpura and Cohen (Purpura & Cohen, 1962)
369 demonstrated that electrical stimulation of the intralaminar nuclei evokes robust excitatory and
370 inhibitory responses in the ventral thalamic nuclei.

371 First-order thalamic neurons express several pH-sensitive ion channels and receptors.
372 TASK-1 and TASK-3, two TWIK-related acid-sensitive potassium channels, with the
373 hyperpolarization-activated cyclic nucleotide–gated (HCN) ion channel, collectively play a critical
374 role in stabilizing the resting membrane potential of first-order thalamic neurons (Meuth et al.,
375 2003, 2006). When activated, TASK channels hyperpolarize the membrane potential of
376 thalamocortical neurons. In contrast, HCN channels depolarize thalamocortical neuron
377 membrane potential. As extracellular acidification inhibits the activity of both channels, the
378 opposing actions of TASK and HCN channels are simultaneously downregulated to yield no net
379 effect on thalamocortical neuron membrane potential (Meuth et al., 2006), thereby stabilizing the
380 membrane potential during acidic conditions. While not yet directly tested, the opposing actions
381 of TASK and HCN channels also presumably stabilize thalamocortical membrane potential
382 during alkaline conditions. Thus, while first-order thalamocortical neurons express pH-sensitive
383 ion channels, these neurons are presumed to maintain stable membrane potentials during
384 extracellular pH fluctuations. If true, then first-order thalamic nuclei are unlikely to support an
385 active role in initiating hyperventilation-provoked spike-wave seizures. The extent to which
386 higher-order thalamic nuclei express TASK and HCH channels remains unknown.

387 Importantly, intralaminar neurons recruited during hyperventilation-mediated alkalosis
388 may not reflect intrinsic pH sensitivity. Instead, activation of intralaminar neurons during
389 alkalosis may result from increased excitatory synaptic input. Intralaminar neurons receive
390 significant, monosynaptic excitation from the midbrain reticular formation (Ropert & Steriade,
391 1981; Steriade & Glenn, 1982); first-order thalamic nuclei only do so negligibly (Edwards & de
392 Olmos, 1976). Several reticular nuclei are critically important for respiration (Guyenet &
393 Bayliss, 2015; Smith et al., 2013) and therefore provide clear rationale for testing the hypothesis
394 that reticular-mediated excitation of the intralaminar nuclei drive hyperventilation-associated
395 cFos expression (i.e., Figure 6). Notably, cFos expression was only observed during respiratory
396 alkalosis (i.e., hypoxia) and not during hyperventilation associated with a normalized arterial pH
397 (i.e., hypoxia-hypercapnia; c.f. Figures 3H and 6B). Thus, if reticular-mediated excitation of
398 intralaminar neurons plays a role in hyperventilation-provoked spike-wave seizures, then it does
399 so only during conditions of respiratory alkalosis. Finally, the possibility that the synaptic
400 terminals of intralaminar-projecting afferents are pH-sensitive also warrants examination.
401 Notably, solute carrier family transporters (SLC) shuttle H^+ and HCO_3^+ across neuronal
402 membranes and are proposed to regulate seizures, including spike-wave seizures (Cox et al.,
403 1997; Sander et al., 2002; Sinning & Hübner, 2013). Alkaline conditions enhance excitatory
404 synaptic transmission, an effect attributed to Slc4a8, a Na^+-Driven Cl^-/Bicarbonate Exchanger
405 (Sinning et al., 2011; Sinning & Hübner, 2013), that is expressed in the presynaptic terminals of
406 excitatory neurons, including those in the thalamus (Lein et al., 2007). Thus, the enhancement
407 of synaptic excitation onto intralaminar neurons remains a plausible mechanism to explain the
408 large excitatory currents activated by alkalinization, as observed in Figure 6F-G. The
409 intralaminar nuclei appear particularly well-suited to transduce alkalization into spike-wave
410 seizures as pH sensitivity within these structures appears heightened relative to other nodes
411 within the spike-wave seizure-generating circuitry (see Figure 6H).
412

413 *Conclusion*

414 In aggregate, our data support the hypothesis that spike-wave seizures are yoked to 415 arterial pH. The observation that respiratory alkalosis activates intralaminar thalamic neurons, 416 and that such neurons are activated by alkaline conditions, reignites a 70-year-old hypothesis 417 wherein intralaminar neurons actively participate in the initiation and maintenance of spike-wave 418 seizures.

419

420

421

422

423 **Material and Methods**

424 Study Design

425 The goal of this study was to parameterize the effect of blood gases on spike-wave 426 seizures. To do so, we adapted a clinically observed human phenomenon in absence epilepsy 427 patients to a rodent model of spike-wave seizures. We demonstrate that spike-wave seizure 428 occurrence correlates with rising or falling values of $PaCO_2$ and pH. Significantly, we show that 429 neurons of the midline thalamus become activated after brief exposure to low $PaCO_2$ conditions. 430 We propose that activity among pH-sensitive neurons in the thalamus, responsive to 431 hyperventilation-induced hypocapnia, trigger spike-wave seizures. All physiology and 432 ECoG/EMG recordings were performed in freely behaving WAG/Rij or Wistar rats. To reduce 433 the number of animals, rats were exposed to multiple conditions. Experimenters were blinded to 434 the condition for all respiration and ECoG/EMG data analysis. Group and sample size were 435 indicated in the results section.

436

437 Animals

438 All procedures conformed to the National Institutes of Health *Guide for Care and Use of*
439 *Laboratory Animals* and were approved by the University of Virginia Animal Care and Use
440 Committee (Charlottesville, VA, USA). Unless otherwise stated, animals were housed at 23-
441 25°C under an artificial 12 h light-dark cycle with food and water *ad libitum*. A colony of Wistar
442 Albino Glaxo/from Rijswik (WAG/Rij rats) were kindly provided by Dr. Edward Bertram,
443 University of Virginia) and maintained in the animal facilities at The University of Virginia
444 Medical Center. Male Wistar IGS Rats were purchased from Charles River (Strain Code: #003).
445 Plethysmography, EEG, blood gas measurements and c-Fos immunohistochemistry
446 experiments were performed in 100+-day old WAG/Rij and Wistar rats as these ages
447 correspond to when spike-wave seizures become robust in the WAG/Rij rat. Male and female
448 rats were used in all experiments – no noticeable differences were observed. Of note, only male
449 rats were used in optogenetic manipulations, as female rats were less likely to recover from
450 surgery.
451
452 Animal Preparation
453 All surgical procedures were conducted under aseptic conditions. Body temperature was
454 maintained at 37°C. Animals were anesthetized with 1-3% isoflurane or a mixture of ketamine
455 (75 mg/kg), xylazine (5 mg/kg) and acepromazine (1 mg/kg) administered intra-muscularly.
456 Depth of anesthesia was monitored by lack of reflex response to a firm toe and tail pinch.
457 Additional anesthetic was administered during surgery (25% of original dose) if warranted. All
458 surgeries, except the arterial catheter implantation, were performed on a stereotaxic frame
459 (David Kopf Instruments, Tujunga, CA, USA). Post-operative antibiotic (ampicillin, 125 mg/kg)
460 and analgesia (ketoprofen, 3-5 mg/kg, subcutaneously) were administered and as needed for 3
461 days. Animals recovered for 1-4 weeks before experimentation.
462
463 Electrocorticogram (ECoG) and electromyography (EMG) electrode implantation

464 Commercially available rat recording devices were purchased from Plastics One
465 (Roanoke, VA, USA). Recording electrodes were fabricated by soldering insulated stainless-
466 steel wire (A-M system, Sequim, WA, USA) to stainless-steel screws (Plastics One) and gold
467 pins (Plastics One). On the day of surgery, a small longitudinal incision was made along the
468 scalp. Small burr holes were drilled in the skill and ECoG recording electrodes were implanted
469 bilaterally in the cortex. Reference electrodes were placed in the cerebellum. A twisted-looped
470 stainless-steel wire was sutured to the superficial neck muscles for EMG recordings. The
471 recording device was secured to the skull with dental cement and incisions were closed with
472 absorbable sutures and/or steel clips.
473

474 PRSX-8 lentivirus preparation

475 The lentivirus, *PRSX8*-hCHR2(H134R)-mCherry, was designed and prepared as
476 described previously (Abbott et al., 2009). Lentivirus vectors were produced by the Salk Institute
477 Viral Vector Core. The titer for the *PRSX8*-hCHR2(H134R)-mCherry lentivirus was diluted to a
478 working concentration of 1.5×10^{10} TU/mL. The same batch of virus was used for all
479 experiments included in this study.
480

481 Virus injection and fiber optic ferrule implantation

482 Borosilicate glass pipettes were pulled to an external tip diameter of 25 μm and
483 backfilled with the lentivirus, *PRSX8*-hCHR2(H134R)-mCherry. Unilateral virus injections in the
484 RTN were made under electrophysiological guidance of the antidromic potential of the facial
485 nucleus (see Abbott et al., 2009; Souza et al., 2018). A total of 400 nL was delivered at three
486 rostro caudal sites separated by 200 or 300 μm in the RTN. Illumination of the RTN was
487 performed by placing a 200-μm-diameter fiber optic (Thor Labs, #BFL37-200; Newton, NJ, USA)
488 and ferrule (Thor Labs, #CFX128-10) vertically through the cerebellum between 300-1000 μm

489 dorsal to RTN ChR2-expressing neurons. These animals were also implanted with ECoG/EMG
490 recording electrodes, as detailed above. All hardware was secured to the skill with dental
491 cement. Animals recovered for 4 weeks, as this provided sufficient time for lentivirus expression
492 in the RTN. Virus injection location was verified post-hoc. Only animals that responded to optical
493 stimulation, demonstrated by an increase in respiratory frequency, were included in the results.
494

495 Physiology experiments in freely behaving rats

496 All experiments were performed during the dark cycle (hours 0-4) at ambient room
497 temperature of 27°C-28°C. Rats were habituated to experimental conditions for a minimum of 4
498 hours, 1-2 d before experiment start. On the day of recordings, rats were briefly anesthetized
499 with 3% isoflurane for < 5min to connect the ECoG/EMG recording head stage to a recording
500 cable and, when necessary, to connect the fiber optic ferrule to a fiber optic cord (multimode
501 200μm core, 0.39 nA) attached to a 473 nm blue laser (CrystaLaser model BC-273-060-M,
502 Reno, NV, USA). Laser power was set to 14mW measured at the junction between the
503 connecting fiber and the rat. Rats were then placed immediately into a whole-body
504 plethysmography chamber (5L, EMKA Technologies, Falls Church, VA, USA). Recordings
505 began after 1 h of habituation. The plethysmography chamber was continuously perfused with
506 room air or protocols cycling through specific gas mixtures of O_2, N_2 and CO_2 (total flow: 1.5
507 L/min). Mass flow controllers, operated by a custom-written Python script, regulated gas
508 exchange. Respiratory flow was recorded with a differential pressure transducer. The
509 respiratory signal was filtered and amplified at 0.1-100 Hz, X 500 (EMKA Technologies).
510 Respiratory signals were digitized at 200 Hz (CED Instruments, Power1401, Cambridge,
511 England). ECoG and EMG signals were amplified (X1000, Harvard Apparatus, Holliston, MA,
512 USA; Model 1700 Differential Amplifier, A-M Systems), bandpass filtered (ECoG: 0.1-100 Hz;
513 EMG: 100-300 Hz) and digitized at 200 Hz. Respiratory flow, ECoG/EMG recordings, O_2 flow
514 and the laser pulse protocol were captured using Spike2, 7.03 software (CED Instruments).

515 Spike-wave seizures were manually identified by blinded individuals. Once identified,
516 custom Matlab scripts identified the true on- and offset of each spike-wave seizure by locating
517 the time point of the first and last peak of the seizure (as defined by sections of the recording
518 that were 2.5 times the pre-seizure RMS baseline); seizure duration was defined as the duration
519 between the first and last peak. Seizure frequency was quantified by computing a fast Fourier
520 transform (FFT) on the event. Spike-wave seizure occurrence before and during specific
521 conditions is shown as a peri-stimulus time histogram aligned at time = 0 at gas exchange onset
522 or laser-on for optogenetic stimulations. Spike-wave seizure counts were quantified in 3 bins
523 beginning +/- 15 minutes of gas exchange or laser onset. Total spike-wave seizure counts were
524 obtained by summing the number of spike-wave seizures between -15 and 0 minutes (control)
525 and 0 and +15 minutes (manipulation). Respiratory frequency (f_R, in breaths/minute) was
526 derived from the respiration trace. The respiration trace was divided into individual windows,
527 each 10 seconds in duration, and a FFT was computed on each discrete window. The
528 respiratory rate for each window was defined by the FFT frequency with the maximal power
529 density. Once derived for each window, we then applied a 30-second moving average to
530 smooth the trace. RTN neurons were optically stimulated with 10 ms pulses delivered at 20 Hz
531 for 2 seconds, followed by 2 seconds rest. This stimulation protocol was repeated for 20
532 minutes.
533

534 Femoral artery catheterization, blood gases and pH measurements.

535 Arterial blood samples for blood gas measurements through an arterial catheter during
536 physiological experiments. One day prior to the experiments, rats anesthetized with isoflurane
537 (2% in pure O_2) and a polyethylene catheter (P-10 to P-50, Clay Adams, Parsippany, NJ, USA)
538 was introduced into the femoral artery by a small skin incision towards the abdominal aorta. The
539 catheter was then tunneled under the skin and exteriorized between the scapulae with two
540 inches of exposed tubing anchored with a suture. On the day of the experiment, animals were

541 briefly anesthetized with 1-2% isoflurane to attach tubing for blood collection before placement
542 into the plethysmography recording chamber. Arterial blood gases and pH were measured using
543 a hand-held iStat configured with CG8+ cartridges (Abbott Instruments, Lake Bluff, USA).
544
545 cFos Histology
546 After exposing WAG/Rij rats to 30 minutes of hypoxia (10% O_2; 90% N_2) or
547 hypoxia/hypercapnia (10% O_2; 5% CO_2; 75% N_2) rats were deeply anesthetized and perfused
548 transcardially with 4% paraformaldehyde (pH 7.4). Brains were removed and post-fixed for 12-
549 16 h at 4 °C. 40μm horizontal sections of the thalamus (D/V depth -5.3 mm to 6.0 mm) were
550 obtained using a Leica VT 1000S microtome (Leica Biostystems, Buffalo Grove, IL, USA) and
551 collected in 0.1 M phosphate buffer (PB) with 0.1% sodium azide (Millipore-Sigma, St. Louis,
552 MO, USA). Sections were then transferred to a 0.1M PB solution containing 20% sucrose for
553 1hr, snap-frozen and transferred to 0.1% sodium borohydride for 15 minutes. Slices were
554 washed 2x in phosphate buffered saline (PBS). All blocking and antibody solutions were
555 prepared in an incubation buffer of 0.1% sodium azide, 0.5% Triton X-100 and 2% normal goat
556 serum. Sections were blocked for 4hrs at room temperature or overnight at 4°C in incubation
557 buffer. Sections were washed 3x with PBS between primary and secondary antibody solutions.
558 Primary antibody solutions containing rabbit anti-cFos (1:2000; Cell Signaling Technology Cat#
559 2250, RRID: AB_2247211, Danvers, MA, USA) and biotin (1:200, Jackson ImmunoResearch,
560 West Grove, PA; RRID: AB_2340595) were prepared in incubation buffer and incubated
561 overnight at 4°C. Sections were then incubated overnight in secondary antibody solutions
562 containing donkey strepavidin-Cy3 (1:1000, Jackson ImmunoResearch; RRID: AB_2337244).
563 Immunohistochemical controls were run in parallel on spare sections by omitting the primary
564 antisera and/or the secondary antisera. Sections from each well were mounted and air-dried
565 overnight. Slides were cover-slipped with VectaShield (VectorLabs, Burlingame, CA) with the
566 addition of a DAPI counterstain. All images were captured with a Z1 Axioimager (Zeiss

567 Microscopy, Thornwood, NY, USA) with computer-driven stage (Neurolucida, software version
568 10; MicroBrightfield, Inc., Colchester, VT, USA). Immunological sections were examined with a
569 10x objective under epifluorescence (Cy3). All sections were captured with similar exposure
570 settings. Images were stored in TIFF format and imported into ImageJ (NIH). Images were
571 adjusted for brightness and contrast to reflect the true rendering as much as possible. To count
572 cFos-positive cells, we utilized the particle analysis tools in ImageJ, and applied a pixel area
573 threshold of varying stringency (0-7px^2). Repeated measures ANOVAs for each treatment and
574 threshold were used for statistical analyses.

575

576 Calcium Imaging

577 pGP-AAV-syn-jGCaMP7s-WPRE (Addgene #104487-AAV9) was stereotaxically delivered to the
578 central median thalamic nucleus in P20-30 rats with sterile microliter calibrated glass pipettes. A
579 picospritzer (Picospritzer III, Parker Hannifin) was used to deliver 100-200 nl of virus. Three
580 weeks later, animals were sacrificed and their brains harvested for acute brain slice preparation.
581 Animals were deeply anesthetized with pentobarbital and then transcardially perfused with an
582 ice-cold protective recovery solution containing the following (in mm): 92 NMDG, 26 NaHCO3,
583 25 glucose, 20 HEPES, 10 MgSO4, 5 Na-ascorbate, 3 Na-pyruvate, 2.5 KCl, 2 thiourea, 1.25
584 NaH2PO4, 0.5 CaCl2, titrated to a pH of 7.3–7.4 with HCl (Ting et al., 2014). Horizontal slices
585 (250 μm) containing the intralaminar thalamic nuclei were cut in ice-cold protective recovery
586 solution using a vibratome (VT1200, Leica Biosystems) and then transferred to protective
587 recovery solution maintained at 32–34°C for 12 min. Brain slices were kept in room temperature
588 artificial cerebrospinal fluid (ACSF) containing (in mm): 3 KCl, 140 NaCl, 10 HEPES, 10
589 Glucose, 2 MgCl2, 2 CaCl2. The solution was bubbled with 100% O2 and the pH was set by
590 adding varied amounts KOH. Fluorescence signals were measured with a spinning disk
591 confocal microscope outfitted with an sCMOS camera (ORCA-Flash4.0, Hamamatsu,
592 Bridgewater, NJ, USA).

593

594 Voltage-Clamp Recordings

595 Brain slices were prepared as described above for calcium imaging experiments; similar ACSF
596 solutions were also used. Thalamic neurons were visualized using a Zeiss Axio Examiner.A1
597 microscope (Zeiss Microscopy, Thornwood, NY, USA) and an sCMOS camera (ORCA-
598 Flash4.0, Hamamatsu). Recording pipettes were pulled on a P1000 puller (Sutter Instruments)
599 from thin-walled borosilicate capillary glass (Sutter Instruments, Novato, CA, USA). Pipettes (2-3
600 MΩ tip resistance) were filled with (in mM) 100 K-gluconate, 9 MgCl2, 13 KCl, 0.07 CaCl2, 10
601 HEPES, 10 EGTA, 2 Na2ATP, 0.5 NaGTP, pH adjusted to 7.3 with KOH, and osmolality
602 adjusted to 275 mOsm. Recordings were performed in the whole cell patch clamp configuration.
603 Data were acquired in pClamp software (Molecular Devices, San Jose, CA, USA) using a
604 Multiclamp 700B amplifier (Molecular Devices), low-pass filtered at 2 kHz, and digitized at 10
605 kHz (Digidata 1440A, Molecular Devices). Access resistance was monitored by repeatedly
606 applying a -5 mV hyperpolarizing voltage step and converting the resultant capacitive transient
607 response into resistance (Ulrich & Huguenard, 1997). A good recording consisted of an access
608 resistance less than 20 MΩ that changed by less than 20% over the course of the recording;
609 recordings that did not meet these criteria were discarded.

610

611 Data analysis and statistics

612 Statistical analyses were performed in GraphPad Prism v7 (San Diego, CA, USA). All
613 data were tested for normality before additional statistical testing. Statistical details, including
614 sample size, are found in the results section and corresponding supplemental tables. Either
615 parametric or non-parametric statistical analyses were performed. A significance level was set
616 at 0.05. Data are expressed as mean ± SEM. Data have been have been deposited at
617 https://doi.org/10.5061/dryad.zcrjdfncm and custom scripts are available at
618 https://github.com/blabuva.

619
620
621
622
623
624
625
626
627
628
629
630
631
632
633

634 **References**

635 Abbott, S. B. G., Stornetta, R. L., Coates, M. B., & Guyenet, P. G. (2011). Phox2b-Expressing Neurons of
636 the Parafacial Region Regulate Breathing Rate, Inspiration, and Expiration in Conscious Rats.
637 *Journal of Neuroscience*, *31*(45), 16410–16422. https://doi.org/10.1523/JNEUROSCI.3280-
638 11.2011

639 Abbott, S. B. G., Stornetta, R. L., Fortuna, M. G., Depuy, S. D., West, G. H., Harris, T. E., & Guyenet, P. G.
640 (2009). Photostimulation of Retrotrapezoid Nucleus Phox2b-Expressing Neurons In Vivo
641 Produces Long-Lasting Activation of Breathing in Rats. *Journal of Neuroscience*, *29*(18), 5806–
642 5819. https://doi.org/10.1523/JNEUROSCI.1106-09.2009

643 Adams, D. J., & Lueders, H. (1981). Hyperventilation and 6-hour EEG recording in evaluation of absence
644 seizures. *Neurology*, *31*(9), 1175–1177. https://doi.org/10.1212/wnl.31.9.1175

645 Amengual-Gual, M., Sánchez Fernández, I., & Loddenkemper, T. (2019). Patterns of epileptic seizure
646 occurrence. *Brain Research*, *1703*, 3–12. https://doi.org/10.1016/j.brainres.2018.02.032

647 Avoli, M. (2012). A brief history on the oscillating roles of thalamus and cortex in absence seizures.
648 *Epilepsia*, *53*(5), 779–789. https://doi.org/10.1111/j.1528-1167.2012.03421.x

649 Bal, T., & McCormick, D. A. (1993). Mechanisms of oscillatory activity in guinea-pig nucleus reticularis
650 thalami in vitro: A mammalian pacemaker. *The Journal of Physiology*, *468*(1), 669–691.
651 https://doi.org/10.1113/jphysiol.1993.sp019794

652 Bal, T., von Krosigk, M., & McCormick, D. A. (1995). Role of the ferret perigeniculate nucleus in the
653 generation of synchronized oscillations in vitro. *The Journal of Physiology*, *483*(3), 665–685.
654 https://doi.org/10.1113/jphysiol.1995.sp020613

655 Banerjee, P. K., & Snead, O. C. (1994). Thalamic mediodorsal and intralaminar nuclear lesions disrupt the
656 generation of experimentally induced generalized absence-like seizures in rats. *Epilepsy*
657 *Research*, *17*(3), 193–205. https://doi.org/10.1016/0920-1211(94)90050-7

658 Barker, A., Ng, J., Rittey, C. D. C., Kandler, R. H., & Mordekar, S. R. (2012). Outcome of children with
659 hyperventilation-induced high-amplitude rhythmic slow activity with altered awareness.
660 *Developmental Medicine and Child Neurology*, *54*(11), 1001–1005.
661 https://doi.org/10.1111/j.1469-8749.2012.04337.x
662 Bartolini, E., & Sander, J. W. (2019). Dealing with the storm: An overview of seizure precipitants and
663 spontaneous seizure worsening in drug-resistant epilepsy. *Epilepsy & Behavior*, *97*, 212–218.
664 https://doi.org/10.1016/j.yebeh.2019.05.036
665 Basting, T. M., Burke, P. G. R., Kanbar, R., Viar, K. E., Stornetta, D. S., Stornetta, R. L., & Guyenet, P. G.
666 (2015). Hypoxia Silences Retrotrapezoid Nucleus Respiratory Chemoreceptors via Alkalosis. *The*
667 *Journal of Neuroscience*, *35*(2), 527–543. https://doi.org/10.1523/jneurosci.2923-14.2015
668 Baud, M. O., Kleen, J. K., Mirro, E. A., Andrechak, J. C., King-Stephens, D., Chang, E. F., & Rao, V. R.
669 (2018). Multi-day rhythms modulate seizure risk in epilepsy. *Nature Communications*, *9*(1), 1–
670 10. https://doi.org/10.1038/s41467-017-02577-y
671 Bazil, C. W. (2019). Seizure modulation by sleep and sleep state. *Brain Research*, *1703*, 13–17.
672 https://doi.org/10.1016/j.brainres.2018.05.003
673 Beenhakker, M. P., & Huguenard, J. R. (2009). Neurons that Fire Together Also Conspire Together: Is
674 Normal Sleep Circuitry Hijacked to Generate Epilepsy? *Neuron*, *62*(5), 612–632.
675 http://dx.doi.org/10.1016/j.neuron.2009.05.015
676 Bezdudnaya, T., & Keller, A. (2008). Laterodorsal Nucleus of the Thalamus: A Processor of
677 Somatosensory Inputs. *The Journal of Comparative Neurology*, *507*(6), 1979–1989.
678 https://doi.org/10.1002/cne.21664
679 Chen, T. T., Klassen, T. L., Goldman, A. M., Marini, C., Guerrini, R., & Noebels, J. L. (2013). Novel brain
680 expression of ClC-1 chloride channels and enrichment of CLCN1 variants in epilepsy. *Neurology*,
681 *80*(12), 1078–1085. https://doi.org/10.1212/WNL.0b013e31828868e7

682 Coenen, A. M. (2003). Genetic animal models for absence epilepsy: A review of the WAG/Rij strain of
683 rats. *Behavior Genetics*, *33*(6), 635–655.
684 Coenen, A. M., Drinkenburg, W. H., Inoue, M., & van Luijtelaar, E. L. (1992). Genetic models of absence
685 epilepsy, with emphasis on the WAG/Rij strain of rats. *Epilepsy Res.*, *12*, 75–86.
686 Cox, G. A., Lutz, C. M., Yang, C.-L., Biemesderfer, D., Bronson, R. T., Fu, A., Aronson, P. S., Noebels, J. L., &
687 Frankel, W. N. (1997). Sodium/Hydrogen Exchanger Gene Defect in Slow-Wave Epilepsy Mutant
688 Mice. *Cell*, *91*(1), 139–148. https://doi.org/10.1016/S0092-8674(01)80016-7
689 Crunelli, V., & Leresche, N. (2002). Childhood absence epilepsy: Genes, channels, neurons and networks.
690 *Nat Rev Neurosci*, *3*(5), 371–382.
691 Debski, K. J., Ceglia, N., Ghestem, A., Ivanov, A. I., Brancati, G. E., Bröer, S., Bot, A. M., Müller, J. A.,
692 Schoch, S., Becker, A., Löscher, W., Guye, M., Sassone-Corsi, P., Lukasiuk, K., Baldi, P., & Bernard,
693 C. (2020). The circadian dynamics of the hippocampal transcriptome and proteome is altered in
694 experimental temporal lobe epilepsy. *Science Advances*, *6*(41), eaat5979.
695 https://doi.org/10.1126/sciadv.aat5979
696 Donevan, R. E., Anderson, N. M., Sekelj, P., Papp, O., & McGregor, M. (1962). Influence of voluntary
697 hyperventilation on cardiac output. *Journal of Applied Physiology*, *17*(3), 487–491.
698 https://doi.org/10.1152/jappl.1962.17.3.487
699 Edwards, S. B., & de Olmos, J. S. (1976). Autoradiographic studies of the projections of the midbrain
700 reticular formation: Ascending projections of nucleus cuneiformis. *The Journal of Comparative*
701 *Neurology*, *165*(4), 417–431. https://doi.org/10.1002/cne.901650403
702 Eldridge, F. L., Kiley, J. P., & Millhorn, D. E. (1984). Respiratory effects of carbon dioxide-induced changes
703 of medullary extracellular fluid pH in cats. *The Journal of Physiology*, *355*, 177–189.
704 https://doi.org/10.1113/jphysiol.1984.sp015413

705 Ferlisi, M., & Shorvon, S. (2014). Seizure precipitants (triggering factors) in patients with epilepsy.
706 *Epilepsy & Behavior: E&B*, *33*, 101–105. https://doi.org/10.1016/j.yebeh.2014.02.019
707 Festing, M. F. W. (1979). Inbred Strains of Rats. In M. F. W. Festing (Ed.), *Inbred Strains in Biomedical*
708 *Research* (pp. 267–296). Macmillan Education UK. https://doi.org/10.1007/978-1-349-03816-
709 9_14
710 Fountain, N. B., Kim, J. S., & Lee, S. I. (1998). Sleep Deprivation Activates Epileptiform Discharges
711 Independent of the Activating Effects of Sleep. *Journal of Clinical Neurophysiology*, *15*(1), 69–75.
712 Guyenet, P. G. (2014). Regulation of Breathing and Autonomic Outflows by Chemoreceptors.
713 *Comprehensive Physiology*, *4*(4), 1511–1562. https://doi.org/10.1002/cphy.c140004
714 Guyenet, P. G., & Bayliss, D. A. (2015). Neural Control of Breathing and CO2 Homeostasis. *Neuron*, *87*(5),
715 946–961. http://dx.doi.org/10.1016/j.neuron.2015.08.001
716 Guyenet, P. G., Bayliss, D. A., Stornetta, R. L., Ludwig, M.-G., Kumar, N. N., Shi, Y., Burke, P. G. R., Kanbar,
717 R., Basting, T. M., Holloway, B. B., & Wenker, I. C. (2016). Proton detection and breathing
718 regulation by the retrotrapezoid nucleus. *The Journal of Physiology*, *594*(6), 1529–1551.
719 https://doi.org/10.1113/JP271480
720 Guyenet, P. G., Stornetta, R. L., Souza, G. M. P. R., Abbott, S. B. G., Shi, Y., & Bayliss, D. A. (2019). The
721 Retrotrapezoid Nucleus: Central Chemoreceptor and Regulator of Breathing Automaticity.
722 *Trends in Neurosciences*, *42*(11), 807–824. https://doi.org/10.1016/j.tins.2019.09.002
723 Helbig, I. (2015). Genetic Causes of Generalized Epilepsies. *Seminars in Neurology*, *35*(03), 288–292.
724 https://doi.org/10.1055/s-0035-1552922
725 Herzog, A. G., & Frye, C. A. (2014). Allopregnanolone levels and seizure frequency in progesterone-
726 treated women with epilepsy. *Neurology*, *83*(4), 345–348.
727 https://doi.org/10.1212/WNL.0000000000000623
728 Holowach, J., Thurston, D., & O'Leary, J. L. (1962). Petit Mal Epilepsy. *Pediatrics*, *30*, 893–901.

729 Hughes, J. R. (2009). Absence seizures: A review of recent reports with new concepts. *Epilepsy &*
730 *Behavior*, *15*(4), 404–412. https://doi.org/10.1016/j.yebeh.2009.06.007
731 Huguenard, J. (2019). Current Controversy: Spikes, Bursts, and Synchrony in Generalized Absence
732 Epilepsy: Unresolved Questions Regarding Thalamocortical Synchrony in Absence Epilepsy.
733 *Epilepsy Currents*, *19*(2), 105–111. https://doi.org/10.1177/1535759719835355
734 Huguenard, J. R., & McCormick, D. A. (2007). Thalamic synchrony and dynamic regulation of global
735 forebrain oscillations. *Trends in Neurosciences*, *30*(7), 350–356.
736 https://doi.org/10.1016/j.tins.2007.05.007
737 Hunter, J., & Jasper, H. H. (1949). Effects of thalamic stimulation in unanaesthetised animals: The arrest
738 reaction and petit Mal-like seizures, activation patterns and generalized convulsions.
739 *Electroencephalography and Clinical Neurophysiology*, *1*(1–4), 305–324.
740 http://dx.doi.org/10.1016/0013-4694(49)90196-0
741 Hwang, D. Y., Carlezon, W. A., Isacson, O., & Kim, K. S. (2001). A high-efficiency synthetic promoter that
742 drives transgene expression selectively in noradrenergic neurons. *Human Gene Therapy*, *12*(14),
743 1731–1740. https://doi.org/10.1089/104303401750476230
744 Jasper, H. H., & Droogleever-Fortuyn, J. (1947). Experimental studies of the functional anatomy of petit
745 mal epilepsy. *Res. Publ. Assoc. Res. Nerve Ment. Dis.*, *26*, 272–298.
746 Joshi, S., & Kapur, J. (2019). Neurosteroid regulation of GABAA receptors: A role in catamenial epilepsy.
747 *Brain Research*, *1703*, 31–40. https://doi.org/10.1016/j.brainres.2018.02.031
748 Kasteleijn-Nolst Trenité, D. G. A. (2012). Provoked and reflex seizures: Surprising or common? *Epilepsia*,
749 *53 Suppl 4*, 105–113. https://doi.org/10.1111/j.1528-1167.2012.03620.x
750 Koeleman, B. P. C. (2018). What do genetic studies tell us about the heritable basis of common epilepsy?
751 Polygenic or complex epilepsy? *Neuroscience Letters*, *667*, 10–16.
752 https://doi.org/10.1016/j.neulet.2017.03.042

753 Koepp, M. J., Caciagli, L., Pressler, R. M., Lehnertz, K., & Beniczky, S. (2016). Reflex seizures, traits, and
754 epilepsies: From physiology to pathology. *The Lancet. Neurology*, *15*(1), 92–105.
755 https://doi.org/10.1016/S1474-4422(15)00219-7
756 Laffey, J. G., & Kavanagh, B. P. (2002). Hypocapnia. *New England Journal of Medicine*, *347*(1), 43–53.
757 https://doi.org/10.1056/NEJMra012457
758 Lein, E. S., Hawrylycz, M. J., Ao, N., Ayres, M., Bensinger, A., Bernard, A., Boe, A. F., Boguski, M. S.,
759 Brockway, K. S., Byrnes, E. J., Chen, L., Chen, L., Chen, T.-M., Chi Chin, M., Chong, J., Crook, B. E.,
760 Czaplinska, A., Dang, C. N., Datta, S., … Jones, A. R. (2007). Genome-wide atlas of gene
761 expression in the adult mouse brain. *Nature*, *445*(7124), 168–176.
762 https://doi.org/10.1038/nature05453
763 Lennox, W. G. (1928). The effect on epileptic seizures of varying composition of respired air. *J. Clin.*
764 *Investigation*, *6*, 23–24.
765 Lindsey, B. G., Nuding, S. C., Segers, L. S., & Morris, K. F. (2018). Carotid Bodies and the Integrated
766 Cardiorespiratory Response to Hypoxia. *Physiology*, *33*(4), 281–297.
767 https://doi.org/10.1152/physiol.00014.2018
768 Lonergan, T., Teschemacher, A. G., Hwang, D. Y., Kim, K.-S., Pickering, A. E., & Kasparov, S. (2005).
769 Targeting brain stem centers of cardiovascular control using adenoviral vectors: Impact of
770 promoters on transgene expression. *Physiological Genomics*, *20*(2), 165–172.
771 https://doi.org/10.1152/physiolgenomics.00120.2004
772 López-Barneo, J., Macías, D., Platero-Luengo, A., Ortega-Sáenz, P., & Pardal, R. (2016). Carotid body
773 oxygen sensing and adaptation to hypoxia. *Pflugers Archiv: European Journal of Physiology*,
774 *468*(1), 59–70. https://doi.org/10.1007/s00424-015-1734-0
775 Lum, L. M., Connolly, M. B., Farrell, K., & Wong, P. K. H. (2002). Hyperventilation-induced High-
776 amplitude Rhythmic Slowing with Altered Awareness: A Video-EEG Comparison with Absence

777 Seizures. *Epilepsia (Series 4)*, *43*(11), 1372–1378. https://doi.org/10.1046/j.1528-
778 1157.2002.35101.x
779 Lusardi, T. A., Akula, K. K., Coffman, S. Q., Ruskin, D. N., Masino, S. A., & Boison, D. (2015). Ketogenic diet
780 prevents epileptogenesis and disease progression in adult mice and rats. *Neuropharmacology*,
781 *99*, 500–509. http://dx.doi.org/10.1016/j.neuropharm.2015.08.007
782 Ma, X., Zhang, Y., Yang, Z., Liu, X., Sun, H., Qin, J., Wu, X., & Liang, J. (2011). Childhood absence epilepsy:
783 Electroclinical features and diagnostic criteria. *Brain and Development*, *33*(2), 114–119.
784 http://dx.doi.org/10.1016/j.braindev.2010.02.004
785 Malow, B. A., Selwa, L. M., Ross, D., & Aldrich, M. S. (1999). Lateralizing value of interictal spikes on
786 overnight sleep-EEG studies in temporal lobe epilepsy. *Epilepsia*, *40*(11), 1587–1592.
787 https://doi.org/10.1111/j.1528-1157.1999.tb02044.x
788 Masino, S. A., Kawamura Jr, M., Ruskin, D. N., Geiger, J. D., & Boison, D. (2012). Purines and neuronal
789 excitability: Links to the ketogenic diet. *Epilepsy Research*, *100*(3), 229–238.
790 http://dx.doi.org/10.1016/j.eplepsyres.2011.07.014
791 Masino, S. A., & Rho, J. M. (2012). Mechanisms of Ketogenic Diet Action. In J. L. Noebels, M. Avoli, M. A.
792 Rogawski, R. W. Olsen, & A. V. Delgado-Escueta (Eds.), *Jasper's Basic Mechanisms of the*
793 *Epilepsies* (4th ed.). National Center for Biotechnology Information (US).
794 http://www.ncbi.nlm.nih.gov/books/NBK98219/
795 Masino, S. A., & Rho, J. M. (2019). Metabolism and epilepsy: Ketogenic diets as a homeostatic link. *Brain*
796 *Research*, *1703*, 26–30. https://doi.org/10.1016/j.brainres.2018.05.049
797 Mattozzi, S., Cerminara, C., Sotgiu, M. A., Carta, A., Coniglio, A., Roberto, D., Simula, D. M., Luca
798 Pruneddu, G., Dell'Avvento, S., Muzzu, S. S., Fadda, M., Luzzu, G. M., Sotgiu, S., & Casellato, S.
799 (2021). Occurrence of hyperventilation-induced high amplitude rhythmic slowing with altered

800 awareness after successful treatment of typical absence seizures and a network hypothesis.
801 *Clinical Neurophysiology Practice*, *6*, 185–188. https://doi.org/10.1016/j.cnp.2021.03.009
802 McCafferty, C., David, F., Venzi, M., Lőrincz, M. L., Delicata, F., Atherton, Z., Recchia, G., Orban, G.,
803 Lambert, R. C., Di Giovanni, G., Leresche, N., & Crunelli, V. (2018). Cortical drive and thalamic
804 feed-forward inhibition control thalamic output synchrony during absence seizures. *Nature*
805 *Neuroscience*, *21*(5), 744–756. https://doi.org/10.1038/s41593-018-0130-4
806 McCormick, D. A., & Contreras, D. (2001). On The Cellular and Network Bases of Epileptic Seizures.
807 *Annual Review of Physiology*, *63*(1), 815–846. https://doi.org/10.1146/annurev.physiol.63.1.815
808 Meeren, H. K. M., Pijn, J. P. M., Van Luijtelaar, E. L. J. M., Coenen, A. M. L., & Lopes da Silva, F. H. (2002).
809 Cortical Focus Drives Widespread Corticothalamic Networks during Spontaneous Absence
810 Seizures in Rats. *The Journal of Neuroscience*, *22*(4), 1480–1495.
811 Meeren, H., van Luijtelaar, G., Lopes da Silva, F., & Coenen, A. (2005). Evolving concepts on the
812 pathophysiology of absence seizures: The cortical focus theory. *Archives of Neurology*, *62*(3),
813 371–376. https://doi.org/10.1001/archneur.62.3.371
814 Meuth, S. G., Budde, T., Kanyshkova, T., Broicher, T., Munsch, T., & Pape, H.-C. (2003). Contribution of
815 TWIK-Related Acid-Sensitive K+ Channel 1 (TASK1) and TASK3 Channels to the Control of Activity
816 Modes in Thalamocortical Neurons. *The Journal of Neuroscience*, *23*(16), 6460–6469.
817 Meuth, S. G., Kanyshkova, T., Meuth, P., Landgraf, P., Munsch, T., Ludwig, A., Hofmann, F., Pape, H.-C., &
818 Budde, T. (2006). Membrane Resting Potential of Thalamocortical Relay Neurons Is Shaped by
819 the Interaction Among TASK3 and HCN2 Channels. *Journal of Neurophysiology*, *96*(3), 1517–
820 1529. https://doi.org/10.1152/jn.01212.2005
821 Nobili, L., Baglietto, M. G., Beelke, M., De Carli, F., Veneselli, E., & Ferrillo, F. (2001). Temporal
822 relationship of generalized epileptiform discharges to spindle frequency activity in childhood

823 absence epilepsy. *Clinical Neurophysiology: Official Journal of the International Federation of*
824 *Clinical Neurophysiology*, *112*(10), 1912–1916. https://doi.org/10.1016/s1388-2457(01)00624-1
825 Padmanaban, V., Inati, S., Ksendzovsky, A., & Zaghloul, K. (2019). Clinical advances in photosensitive
826 epilepsy. *Brain Research*, *1703*, 18–25. https://doi.org/10.1016/j.brainres.2018.07.025
827 Paxinos, G., & Watson, C. (2007). *The Rat Brain In Sterotaxic Coordinates* (6th ed.). Elsevier.
828 Paz, J. T., & Huguenard, J. R. (2015). Microcircuits and their interactions in epilepsy: Is the focus out of
829 focus? *Nat Neurosci*, *18*(3), 351–359. https://doi.org/10.1038/nn.3950
830 Pinault, D. (2003). Cellular interactions in the rat somatosensory thalamocortical system during normal
831 and epileptic 5–9 Hz oscillations. *The Journal of Physiology*, *552*(3), 881–905.
832 https://doi.org/10.1113/jphysiol.2003.046573
833 Pinault, D., Leresche, N., Charpier, S., Deniau, J.-M., Marescaux, C., Vergnes, M., & Crunelli, V. (1998).
834 Intracellular recordings in thalamic neurones during spontaneous spike and wave discharges in
835 rats with absence epilepsy. *The Journal of Physiology*, *509*(2), 449–456.
836 https://doi.org/10.1111/j.1469-7793.1998.449bn.x
837 Purpura, D. P., & Cohen, B. (1962). Intracellular recording from thalamic neurons during recruiting
838 responses. *Journal of Neurophysiology*, *25*(5), 621–635.
839 https://doi.org/10.1152/jn.1962.25.5.621
840 Raichle, M. E., & Plum, F. (1972). Hyperventilation and Cerebral Blood Flow. *Stroke*, *3*(5), 566–575.
841 https://doi.org/10.1161/01.STR.3.5.566
842 Reddy, D. S., Kim, H.-Y., & Rogawski, M. A. (2001). Neurosteroid Withdrawal Model of Perimenstrual
843 Catamenial Epilepsy. *Epilepsia*, *42*(3), 328–336. https://doi.org/10.1046/j.1528-
844 1157.2001.10100.x

845 Robinson, P. F., & Gilmore, S. A. (1980). Spontaneous generalized spike-wave discharges in the
846 electrocorticograms of albino rats. *Brain Research*, *201*(2), 452–458.
847 https://doi.org/10.1016/0006-8993(80)91052-5
848 Robinson, R., Taske, N., Sander, T., Heils, A., Whitehouse, W., Goutières, F., Aicardi, J., Lehesjoki, A.-E.,
849 Siren, A., Laue Friis, M., Kjeldsen, M. J., Panayiotopoulos, C., Kennedy, C., Ferrie, C., Rees, M., &
850 Gardiner, R. M. (2002). Linkage analysis between childhood absence epilepsy and genes
851 encoding GABAA and GABAB receptors, voltage-dependent calcium channels, and the ECA1
852 region on chromosome 8q. *Epilepsy Research*, *48*(3), 169–179. https://doi.org/10.1016/S0920-
853 1211(01)00335-7
854 Ropert, N., & Steriade, M. (1981). Input-output organization of midbrain reticular core. *Journal of*
855 *Neurophysiology*, *46*(1), 17–31. https://doi.org/10.1152/jn.1981.46.1.17
856 Russo, E., Citraro, R., Constanti, A., Leo, A., Lüttjohann, A., van Luijtelaar, G., & De Sarro, G. (2016).
857 Upholding WAG/Rij rats as a model of absence epileptogenesis: Hidden mechanisms and a new
858 theory on seizure development. *Neuroscience & Biobehavioral Reviews*, *71*, 388–408.
859 https://doi.org/10.1016/j.neubiorev.2016.09.017
860 Saalmann, Y. B. (2014). Intralaminar and medial thalamic influence on cortical synchrony, information
861 transmission and cognition. *Frontiers in Systems Neuroscience*, *8*.
862 https://doi.org/10.3389/fnsys.2014.00083
863 Sadleir, L. G., Farrell, K., Smith, S., Connolly, M. B., & Scheffer, I. E. (2006). Electroclinical features of
864 absence seizures in childhood absence epilepsy. *Neurology*, *67*(3), 413.
865 https://doi.org/10.1212/01.wnl.0000228257.60184.82
866 Sadleir, L. G., Scheffer, I. E., Smith, S., Carstensen, B., Carlin, J., Connolly, M. B., & Farrell, K. (2008).
867 Factors influencing clinical features of absence seizures. *Epilepsia*, *49*(12), 2100–2107.
868 https://doi.org/10.1111/j.1528-1167.2008.01708.x

869 Sadleir, L. G., Scheffer, I., Smith, S., Carstensen, B., Farrell, K., & Connolly, M. B. (2009). EEG features of
870 absence seizures in idiopathic generalized epilepsy: Impact of syndrome, age, and state.
871 *Epilepsia*, *50*(6), 1572–1578. https://doi.org/10.1111/j.1528-1167.2008.02001.x
872 Sander, T., Toliat, M. R., Heils, A., Leschik, G., Becker, C., Rüschendorf, F., Rohde, K., Mundlos, S., &
873 Nürnberg, P. (2002). Association of the 867Asp variant of the human anion exchanger 3 gene
874 with common subtypes of idiopathic generalized epilepsy. *Epilepsy Research*, *51*(3), 249–255.
875 https://doi.org/10.1016/S0920-1211(02)00152-3
876 Sarrigiannis, P. G., Zhao, Y., He, F., Billings, S. A., Baster, K., Rittey, C., Yianni, J., Zis, P., Wei, H.,
877 Hadjivassiliou, M., & Grünewald, R. (2018). The cortical focus in childhood absence epilepsy;
878 evidence from nonlinear analysis of scalp EEG recordings. *Clinical Neurophysiology*, *129*(3), 602–
879 617. https://doi.org/10.1016/j.clinph.2017.11.029
880 Semenza, G. L., & Prabhakar, N. R. (2018). The role of hypoxia-inducible factors in carotid body (patho)
881 physiology. *The Journal of Physiology*, *596*(15), 2977–2983. https://doi.org/10.1113/JP275696
882 Sherwin, I. (1965). Differential effects of hyperventillation on the excitability of intact and isolated
883 cortex. *Electroencephalography and Clinical Neurophysiology*, *18*(6), 599–607.
884 https://doi.org/10.1016/0013-4694(65)90077-5
885 Sherwin, I. (1967). Alterations in the non-specific cortical afference during hyperventilation.
886 *Electroencephalography and Clinical Neurophysiology*, *23*(6), 532–538.
887 https://doi.org/10.1016/0013-4694(67)90019-3
888 Sinning, A., & Hübner, C. A. (2013). Minireview: PH and synaptic transmission. *FEBS Letters*, *587*(13),
889 1923–1928. https://doi.org/10.1016/j.febslet.2013.04.045
890 Sinning, A., Liebmann, L., Kougioumtzes, A., Westermann, M., Bruehl, C., & Hubner, C. A. (2011).
891 Synaptic Glutamate Release Is Modulated by the Na+-Driven Cl-/HCOFormula Exchanger Slc4a8.
892 *Journal of Neuroscience*, *31*(20), 7300–7311. https://doi.org/10.1523/JNEUROSCI.0269-11.2011

893 Smith, J. C., Abdala, A. P. L., Borgmann, A., Rybak, I. A., & Paton, J. F. R. (2013). Brainstem respiratory
894 networks: Building blocks and microcircuits. *Trends in Neurosciences*, *36*(3), 152–162.
895 https://doi.org/10.1016/j.tins.2012.11.004
896 Smyk, M. K., & van Luijtelaar, G. (2020). Circadian Rhythms and Epilepsy: A Suitable Case for Absence
897 Epilepsy. *Frontiers in Neurology*, *11*. https://doi.org/10.3389/fneur.2020.00245
898 Souza, G. M. P. R., Kanbar, R., Stornetta, D. S., Abbott, S. B. G., Stornetta, R. L., & Guyenet, P. G. (2018).
899 Breathing regulation and blood gas homeostasis after near complete lesions of the
900 retrotrapezoid nucleus in adult rats. *The Journal of Physiology*, *596*(13), 2521–2545.
901 https://doi.org/10.1113/JP275866
902 Souza, G. M. P. R., Stornetta, R. L., Stornetta, D. S., Abbott, S. B. G., & Guyenet, P. G. (2019). Contribution
903 of the Retrotrapezoid Nucleus and Carotid Bodies to Hypercapnia- and Hypoxia-induced Arousal
904 from Sleep. *The Journal of Neuroscience: The Official Journal of the Society for Neuroscience*,
905 *39*(49), 9725–9737. https://doi.org/10.1523/JNEUROSCI.1268-19.2019
906 Souza, G. M. P. R., Stornetta, R. L., Stornetta, D. S., Abbott, S. B. G., & Guyenet, P. G. (2020). Differential
907 Contribution of the Retrotrapezoid Nucleus and C1 Neurons to Active Expiration and Arousal in
908 Rats. *The Journal of Neuroscience: The Official Journal of the Society for Neuroscience*, *40*(45),
909 8683–8697. https://doi.org/10.1523/JNEUROSCI.1006-20.2020
910 Steriade, M., & Glenn, L. L. (1982). Neocortical and caudate projections of intralaminar thalamic neurons
911 and their synaptic excitation from midbrain reticular core. *Journal of Neurophysiology*, *48*(2),
912 352–371. https://doi.org/10.1152/jn.1982.48.2.352
913 Stirling, R. E., Cook, M. J., Grayden, D. B., & Karoly, P. J. (2021). Seizure forecasting and cyclic control of
914 seizures. *Epilepsia*, *62*(S1), S2–S14. https://doi.org/10.1111/epi.16541

915 Swanson, L. W., Sporns, O., & Hahn, J. D. (2019). The network organization of rat intrathalamic
916 macroconnections and a comparison with other forebrain divisions. *Proceedings of the National*
917 *Academy of Sciences*, *116*(27), 13661–13669. https://doi.org/10.1073/pnas.1905961116
918 Taylor, J. A., Reuter, J. D., Kubiak, R. A., Mufford, T. T., Booth, C. J., Dudek, F. E., & Barth, D. S. (2019).
919 Spontaneous Recurrent Absence Seizure-like Events in Wild-Caught Rats. *Journal of*
920 *Neuroscience*, *39*(24), 4829–4841. https://doi.org/10.1523/JNEUROSCI.1167-18.2019
921 Taylor, J. A., Rodgers, K. M., Bercum, F. M., Booth, C. J., Dudek, F. E., & Barth, D. S. (2017). Voluntary
922 Control of Epileptiform Spike–Wave Discharges in Awake Rats. *The Journal of Neuroscience*,
923 *37*(24), 5861–5869. https://doi.org/10.1523/JNEUROSCI.3235-16.2017
924 Ting, J. T., Daigle, T. L., Chen, Q., & Feng, G. (2014). Acute Brain Slice Methods for Adult and Aging
925 Animals: Application of Targeted Patch Clamp Analysis and Optogenetics. In M. Martina & S.
926 Taverna (Eds.), *Patch-Clamp Methods and Protocols* (pp. 221–242). Springer New York.
927 https://doi.org/10.1007/978-1-4939-1096-0_14
928 Tyvaert, L., Chassagnon, S., Sadikot, A., LeVan, P., Dubeau, F., & Gotman, J. (2009). Thalamic nuclei
929 activity in idiopathic generalized epilepsy: An EEG-fMRI study. *Neurology*, *73*(23), 2018–2022.
930 https://doi.org/10.1212/WNL.0b013e3181c55d02
931 Ulrich, D., & Huguenard, J. R. (1997). Nucleus-Specific Chloride Homeostasis in Rat Thalamus. *The*
932 *Journal of Neuroscience*, *17*(7), 2348–2354.
933 van Luijtelaar, E. L., & Coenen, A. M. (1986). Two types of electrocortical paroxysms in an inbred strain
934 of rats. *Neuroscience Letters*, *70*(3), 393–397.
935 Vergnes, M., Marescaux, Ch., Micheletti, G., Reis, J., Depaulis, A., Rumbach, L., & Warter, J. M. (1982).
936 Spontaneous paroxysmal electroclinical patterns in rat: A model of generalized non-convulsive
937 epilepsy. *Neuroscience Letters*, *33*(1), 97–101. https://doi.org/10.1016/0304-3940(82)90136-7

938 von Krosigk, M., Bal, T., & McCormick, D. (1993). Cellular mechanisms of a synchronized oscillation in the
939 thalamus. *Science*, *261*(5119), 361. https://doi.org/10.1126/science.8392750
940 Watemberg, N., Farkash, M., Har-Gil, M., Sezer, T., Goldberg-Stern, H., & Alehan, F. (2015).
941 Hyperventilation During Routine Electroencephalography: Are Three Minutes Really Necessary?
942 *Pediatric Neurology*, *52*(4), 410–413. http://dx.doi.org/10.1016/j.pediatrneurol.2014.12.003
943 Xie, H., Su, W., Pei, J., Zhang, Y., Gao, K., Li, J., Ma, X., Zhang, Y., Wu, X., & Jiang, Y. (2019). De novo
944 SCN1A, SCN8A, and CLCN2 mutations in childhood absence epilepsy. *Epilepsy Research*, *154*, 55–
945 61. https://doi.org/10.1016/j.eplepsyres.2019.04.005
946 Yang, X.-F., Shi, X.-Y., Ju, J., Zhang, W.-N., Liu, Y.-J., Li, X.-Y., & Zou, L.-P. (2014). 5% CO2 inhalation
947 suppresses hyperventilation-induced absence seizures in children. *Epilepsy Research*, *108*(2),
948 345–348. http://dx.doi.org/10.1016/j.eplepsyres.2013.11.012

949
950
951

952

953 **Figure Legends**

954

955 **Figure 1. Hypoxia provokes hyperventilation-associated spike-wave seizures in WAG/Rij**
956 **rats.**
957 **(A)** Experimental approach. *Left:* Plethysmography chambers recorded ventilation and
958 ECoG/EMG signals in rats exposed to normoxia (i.e., 21% O_2) and hypoxia (i.e., 10% O_2).
959 *Right:* Example gas exchange protocol used to generate the peristimulus time histogram in
960 panel C. Spike-wave seizure count was measured during the 15 minutes before and after gas
961 exchange at t = 0 min. **(B)** Representative recordings during transition from normoxia to
962 hypoxia. (1) From top to bottom: chamber O_2, respiration, ECoG, EMG, and ECoG power
963 spectrogram. White arrow points to spike-wave seizure. (2) *Bottom:* expanded view B1.
964 Spectrogram reveals 5-8 Hz frequency harmonics associated with spike-wave seizures. **(C)**
965 Spike-wave seizure (SWS) and respiration quantification. (1) Stacked histogram illustrating
966 spike-wave seizure count for each animal before and after the onset of hypoxia; each color is a
967 different rat. Arrow points to gas exchange at t = 0 min. (2) Corresponding respiratory rate for
968 each animal shown in panel C1. (3) Mean respiratory rate for all animals. **(D)** Mean spike-wave
969 seizure count per bin and **(E)** respiratory rate before and after gas exchange. See **Tables 1 & 4**
970 for detailed statistics. ***p < 0.001.

971

972

973

974 **Figure 2. Hypoxia does not provoke hyperventilation-associated spike-wave seizures in**
975 **Wistar rats.**
976 **(A)** Plethysmography chambers recorded ventilation and ECoG/EMG signals in four Wistar rats
977 exposed to normoxia (i.e., 21% O_2) and hypoxia (i.e., 10% O_2). Panels 1-4 include responses

978 from four Wistar rats, respectively, and show from top to bottom: ECoG, ECoG power
979 spectrogram, respiratory rate, and chamber O_2. During the 2.5-hour recording session, rats
980 were challenged twice with hypoxia. No spike-wave seizures were observed during either
981 normoxia or hypoxia. **(B)** Expanded views of the first transition from normoxia to hypoxia shown
982 in panel A. Increased low frequency power during normoxia in some rats (e.g., panel B2)
983 represents sleep. Hypoxia in Wistar rats generally increased arousal. **(C)** Arterial measurements
984 in the same rats show that hypoxia challenges produced a predictable drop in arterial (1) O_2 and
985 (2) CO_2, as well as (3) alkalosis. See **Table 5** for detailed statistics. ***$p < 0.001$.
986
987
988
989 **Figure 3. Supplemental CO_2 suppresses hypoxia-provoked spike-wave seizures.**
990 **(A)** Experimental approach. Plethysmography chambers recorded ventilation and ECoG/EMG
991 signals in WAG/Rij rats exposed to normoxia (i.e., 21% O_2) and then alternately challenged with
992 hypoxia (i.e., 10% O_2) or hypoxia + CO_2, (i.e., 10% O_2, 5% CO_2). **(B-D)** Hypoxia challenge. **(B)**
993 Spike-wave seizure (SWS) and respiration quantification. (1) Stacked histogram illustrating
994 spike-wave seizure count for each animal before and after the onset of hypoxia. (2)
995 Corresponding respiratory rate for each animal shown in panel B1. (3) Mean respiratory rate for
996 all animals. **(C)** Mean spike-wave seizure count per bin and **(D)** respiratory rate before and after
997 hypoxia exchange. **(E-G)** Hypoxia + CO_2 challenge. **(E)** SWS and respiration quantification. (1)
998 Stacked histogram illustrating spike-wave seizure count for each animal before and after the
999 onset of hypoxia + CO_2. (2) Corresponding respiratory rate for each animal shown in panel E1.
1000 (3) Mean respiratory rate for all animals. **(F)** Mean spike-wave seizure count per bin and **(G)**
1001 respiratory rate before after hypoxia + CO_2 exchange. **(H)** Arterial measurements show that
1002 hypoxia produced a predictable drop in arterial (1) O_2 and (2) CO_2, as well as (3) respiratory
1003 alkalosis (as in Wistar rats). Supplementing the chamber with 5% CO_2 normalizes arterial CO_2

1004 and pH. Elevated arterial O_2 during hypoxia + CO_2 relative to hypoxia reflects a powerful
1005 inhalation response during the former condition (c.f., panels D and G). See **Tables 1, 4 and 6**
1006 for detailed statistics. **p<0.01, ***p < 0.001.

1007

1008

1009

1010 **Figure 4. Supplemental CO_2 suppresses spontaneous spike-wave seizures.**
1011 **(A)** Experimental approach. Plethysmography chambers recorded ventilation and ECoG/EMG
1012 signals in WAG/Rij rats exposed to normoxia (i.e., 21% O_2) and hypercapnia (i.e., 21% O_2, 5%
1013 CO_2). **(B)** Spike-wave seizure (SWS) and respiratory quantification. (1) Stacked histogram
1014 illustrating spike-wave seizure count for each animal before and after the onset of hypercapnia.
1015 (2) Corresponding respiratory rate for each animal shown in panel B1. (3) Mean respiratory rate
1016 for all animals. **(C)** Mean spike-wave seizure count per bin and **(D)** respiratory rate before and
1017 after hypercapnia exchange. **(E)** Arterial measurements in the same rats show that hypercapnia
1018 produced a predictable increase in arterial (1) O_2 and (2) CO_2, as well as (3) respiratory
1019 acidosis. Increase arterial O_2 reflects robust ventilatory response during hypercapnia. See
1020 **Tables 1, 4 and 6** for detailed statistics. *p < 0.05, **p < 0.01, ***p < 0.001.

1021

1022

1023

1024 **Figure 5. Normoxic hyperventilation provokes CO_2-sensitive spike-wave seizures. (A)**
1025 Channelrhodopsin was virally delivered to the retrotrapezoid nucleus. The fiber optic cable was
1026 implanted during the surgery. After three weeks, photostimulation of the retrotrapezoid nucleus
1027 induced hyperventilation. **(B)** After experimentation, opsin expression and fiber optic placement
1028 was verified. Representative image of mCherry-positive cells in the retrotrapezoid nucleus.

1029 Large notch in slice is from optical fiber. Box on left image is enlarged on right image. Scale bar
1030 = 500 μm. **(C)** Experimental approach. Plethysmography chambers recorded ventilation and
1031 ECoG/EMG signals in WAG/Rij rats exposed to normoxia (i.e., 21% O_2) and normoxia + CO_2,
1032 (i.e., 10% O_2, 5% CO_2). Channelrhodopsin-mediated photostimulation of the retrotrapezoid
1033 nucleus (RTN) was used to increase ventilation. **(D)** Example of ventilatory response and spike-
1034 wave seizure during normoxic RTN photostimulation. **(E-G)** RTN photostimulation during
1035 normoxia. **(E)** Spike-wave seizure (SWS) and respiration quantification. (1) Stacked histogram
1036 illustrating spike-wave seizure count for each animal before and after normoxia photostimulation
1037 onset. (2) Corresponding respiratory rate for each animal shown in panel C1. (3) Mean
1038 respiratory rate for all animals. **(F)** Mean spike-wave seizure count per bin and **(G)** respiration
1039 rate before and after normoxia photostimulation onset. **(H-J)** RTN photostimulation during
1040 hypercapnia (i.e., 21% O_2, 5% CO_2). **(H)** Spike-wave seizure and respiratory quantification. (1)
1041 Stacked histogram illustrating spike-wave seizure count for each animal before and after
1042 hypercapnic photostimulation onset. (2) Corresponding respiratory rate for each animal shown
1043 in panel F1. (3) Mean respiratory rate for all animals. **(I)** Mean spike-wave seizure count per bin
1044 and **(J)** respiratory rate before and after hypercapnic photostimulation onset. See **Tables 1, 4**
1045 **and 6** for detailed statistics. *p < 0.05, **p < 0.01, not significant (n.s.).
1046
1047
1048
1049 **Figure 6. Hypoxia-induced hyperventilation activates intralaminar thalamic neurons.**
1050 **(A)** cFos immunohistochemistry in horizontal sections of the WAG/Rij rat. Dashed lines highlight
1051 the medial region of the thalamus containing the intralaminar nuclei. Solid lines demarcate
1052 regions containing elevated cFos expression and are expanded on right. Top images are
1053 collected from a rat exposed to 30 minutes of normoxia. Middle images are collected from a rat
1054 exposed to 30 minutes of hypoxia. Bottom images are taken from Paxinos and Watson (Paxinos

1055 & Watson, 2007) and show the structural landmarks in the top and middle images. The central
1056 median nucleus (CM, intralaminar thalamus) and ventrobasal complex (VB, first-order thalamus)
1057 are labeled. **(B)** cFos density plots show immunoreactivity in each of four rats exposed to either
1058 normoxia, hypoxia or hypoxia + CO_2. Each black dot represents a cFos-positive cell, as
1059 identified with ImageJ (see Methods). Plots are aligned to expanded views in panel A. **(C)**
1060 Quantification of cFos labeled cells at different ImageJ thresholding values. **(D)** GCaMP7 was
1061 stereotaxically delivered to the intralaminar nuclei. Later, fluorescence changes were measured
1062 during extracellular alkaline challenges in acute slices containing the intralaminar nuclei.
1063 Individual ROIs show fluorescence changes during alkalosis (black traces). Mean responses
1064 from two animals are shown in green. The lag in response reflects the duration required for a
1065 complete solution exchange. **(E)** pH sensitivity of intralaminar neurons was also evaluated
1066 using electrophysiological measurements in acute brain slices. **(F)** Voltage-clamped intralaminar
1067 neurons (V_{hold} = -50mV) were exposed to control (pH 7.3), alkaline (pH 8.0) and acidic (pH 7.0)
1068 conditions. Inward currents were evoked during alkaline conditions. **(G)** Population intralaminar
1069 neuron response to alkaline conditions (n=5). **(H)** Alkaline-evoked inward currents were largest
1070 in the intralaminar neurons (−146 ± 41.1 pA, n = 5), relative to similar measurements in neurons
1071 of the somatosensory cortex (S1, −59.1 ± 7.3 pA, n = 5) or thalamus (VB, ventrobasal nucleus,
1072 −68.1 ± 3.5 pA, n = 4). Inward currents during alkaline conditions (pH 8.0) in both intralaminar
1073 and S1 neurons were significantly larger, relative to their respective currents measured at a
1074 baseline pH of 7.3. Currents are presented as baseline-subtracted. **$p < 0.01$, ***$p < 0.001$.
1075 See **Table 7** for detailed statistics. Scale bars are 500 μm (*left*) and 100 μm *(right)*.

1076

1077

1078

1079 **Figure 7.** Working model. **A.** Spike-wave seizures only occur if initiating activity from S1
1080 somatosensory cortex successfully overcomes a threshold, consistent with the cortical focus
1081 theory (H. K. M. Meeren et al., 2002). Hyperventilation-associated alkalosis reduces spike-wave
1082 seizure (SWS) threshold. **B.** S1 initiating activity is proposed to overcome a seizure node
1083 formed by circuits in reticular thalamus to generate an spike-wave seizure (Paz & Huguenard,
1084 2015). We propose that hyperventilation-evoked respiratory alkalosis activates the intralaminar
1085 nuclei (ILM) to reduce the threshold for S1 activity required to evoke a spike-wave seizure.
1086 *Thalamic pH sensitivity*
1087

Tables

Table 1. Spike-wave seizure count.

Figure	Comparison	Bin Count (Mean ± S.E.)	n	p value
1D	Normoxia Hypoxia	0.89 ± 0.12 1.73 ± 0.13	15	4.5×10^{-7}
3C	Normoxia Hypoxia	0.99 ± 0.18 1.82 ± 0.14	9	1.76×10^{-6}
3F	Normoxia Hypoxia + CO_2	1.09 ± 0.22 0.84 ± 0.13	9	0.18
4C	Normoxia Normoxia + CO_2	1.36 ± 0.17 0.95 ± 0.10	8	0.0028
5D	Normoxia Normoxia + Photostim.	1.17 ± 0.38 2.27 ± 0.63	10	0.002
5G	Normoxia Normoxia + Photostim.+ CO_2	1.04 ± 0.32 1.01 ± 0.30	6	0.86

Table 2. Spike-wave seizure duration.

Figure	Comparison	Duration (sec) (Mean ± S.E.)	n	p value
1D	Normoxia Hypoxia	5.3 ± 0.4 5.8 ± 0.4	15	0.56
3C	Normoxia Hypoxia	5.5 ± 0.5 6.3 ± 0.5	9	0.26
3F	Normoxia Hypoxia + CO_2	5.5 ± 0.6 7.5 ± 1.0	9	0.006
4C	Normoxia Normoxia + CO_2	5.6 ± 0.4 6.2 ± 0.4	8	0.21
5D	Normoxia Normoxia + Photostim.	4.3 ± 0.6 4.6 ± 0.5	10	0.51
5G	Normoxia Normoxia + Photostim.+ CO_2	6.8 ± 1.0 6.9 ± 1.0	6	0.88

Table 3. Spike-wave seizure frequency.

Figure	Comparison	Frequency (Hz) (Mean ± S.E.)	n	p value
1D	Normoxia Hypoxia	7.6 ± 0.1 5.8 ± 0.4	15	4.7×10^{-5}
3C	Normoxia Hypoxia	7.7 ± 0.2 6.3 ± 0.5	9	0.014
3F	Normoxia Hypoxia + CO_2	7.8 ± 0.1 7.5 ± 1.0	9	0.18
4C	Normoxia Normoxia + CO_2	6.1 ± 1.0 6.2 ± 0.	8	0.28
5D	Normoxia Normoxia + Photostim.	7.5 ± 0.2 4.6 ± 0.5	10	2.2×10^{-4}
5G	Normoxia Normoxia + Photostim.+ CO_2	7.9 ± 0.2 6.9 ± 1.0	6	0.33

Table 4. Respiratory Rate.

Figure	Comparison	Resp. Rate (Hz) (Mean ± S.E.)	n	p value
1E	Normoxia Hypoxia	1.03 ± 0.02 1.33 ± 0.05	15	1.67×10^{-5}
3D	Normoxia Hypoxia	1.00 ± 0.02 1.28 ± 0.05	9	6.59×10^{-4}
3G	Normoxia Hypoxia + CO_2	1.06 ± 0.03 1.88 ± 0.15	9	2.71×10^{-4}
4D	Normoxia Normoxia + CO_2	0.99 ± 0.03 1.78 ± 0.10	9	3.78×10^{-5}
5E	Normoxia Normoxia + Photostim.	1.02 ± 0.03 1.24 ± 0.08	10	0.019
5H	Normoxia Normoxia + Photostim.+ CO_2	1.01 ± 0.03 1.84 ± 0.08	6	0.031

1175
1176
1177 **Table 5. Arterial measurements in Wistar rats.**

Figure	Parameter	Comparison	Value	n	p value
2C1	PaO_2	Normoxia Hypoxia	83.25 ± 2.32 32.25 ± 1.25	4	0.0002
2C2	$PaCO_2$	Normoxia Hypoxia	37.0 ± 0.59 22.33 ± 0.16	4	6.6×10^{-5}
2C3	pH	Normoxia Hypoxia	7.47 ± 0.01 7.63 ± 0.01	4	4.5×10^{-5}

1178
1179
1180
1181
1182
1183
1184
1185 **Table 6. Arterial measurements in WAG/Rij rats.**

Figure	Parameter	Comparison	Value	n	p value
3H1	PaO_2	Normoxia Hypoxia	84.93 ± 1.82 34.50 ± 0.56	6	6.0×10^{-6}

1186
1187
1188

		Normoxia Hypoxia +CO_2	84.93 ± 0.02 55.83 ± 0.87	6	0.000134
3H2	$PaCO_2$	Normoxia Hypoxia	43.48 ± 0.47 25.83 ± 0.65	6	2.1×10^{-6}
		Normoxia Hypoxia +CO_2	43.48 ± 0.47 44.60 ± 0.55	6	0.42
3H3	pH	Normoxia Hypoxia	7.45 ± 0.01 7.61 ± 0.01	6	7.0×10^{-6}
		Normoxia Hypoxia +CO_2	7.45 ± 0.01 7.43 ± 0.01	6	0.008
4E1	PaO_2	Normoxia 5% CO2	84.93 ± 1.82 34.50 ± 0.56	6	0.00019
4E2	$PaCO_2$	Normoxia 5% CO2	43.48 ± 0.47 25.83 ± 0.65	6	0.022
4E3	pH	Normoxia 5% CO2	7.45 ± 0.01 7.42 ± 0.01	6	0.00063

1189
1190
1191
1192
1193

Table 7. cFos-positive cells in WAG/Rij rats.

Figure	Threshold	Comparison	Counts (Mean ± S.E.)	n	p value
6C	3	Normoxia Hypoxia	282 ± 148.2 1370 ± 137	4	1.5×10^{-7}
		Normoxia Hypoxia + CO2	282 ± 148.2 385.5 ± 78.7	4	0.55
		Hypoxia Hypoxia + CO2	1370 ± 137 385.5 ± 78.7	4	4.3×10^{-7}
	5	Normoxia Hypoxia	112.3 ± 57.1 595.3 ± 85.0	4	0.0005
		Normoxia Hypoxia + CO2	112.3 ± 57.1 348 ± 68.9	4	0.045
		Hypoxia Hypoxia + CO2	595.3 ± 85.0 348 ± 68.9	4	0.061
	7	Normoxia Hypoxia	57.3 ± 29.2 349 ± 75.0	4	0.021
		Normoxia Hypoxia + CO2	57.3 ± 29.2 319.5 ± 63.1	4	0.036
		Hypoxia Hypoxia + CO2	349 ± 75.0 319.5 ± 63.1	4	0.95
			Holding Currents (pA)	**n**	**p value**
6H	Intra	Baseline pH 7.3 pH 8.0	9.9 ± 11.1 -136.6 ± 17.5	5	0.016
	S1	Baseline pH 7.3 pH 8.0	-4.2 ± 5.3 -63.3 ± 8.4	5	.008
	VB	Baseline pH 7.3 pH 8.0	6.5 ± 19.4 -61.6 ± 27.4	4	.057

1226

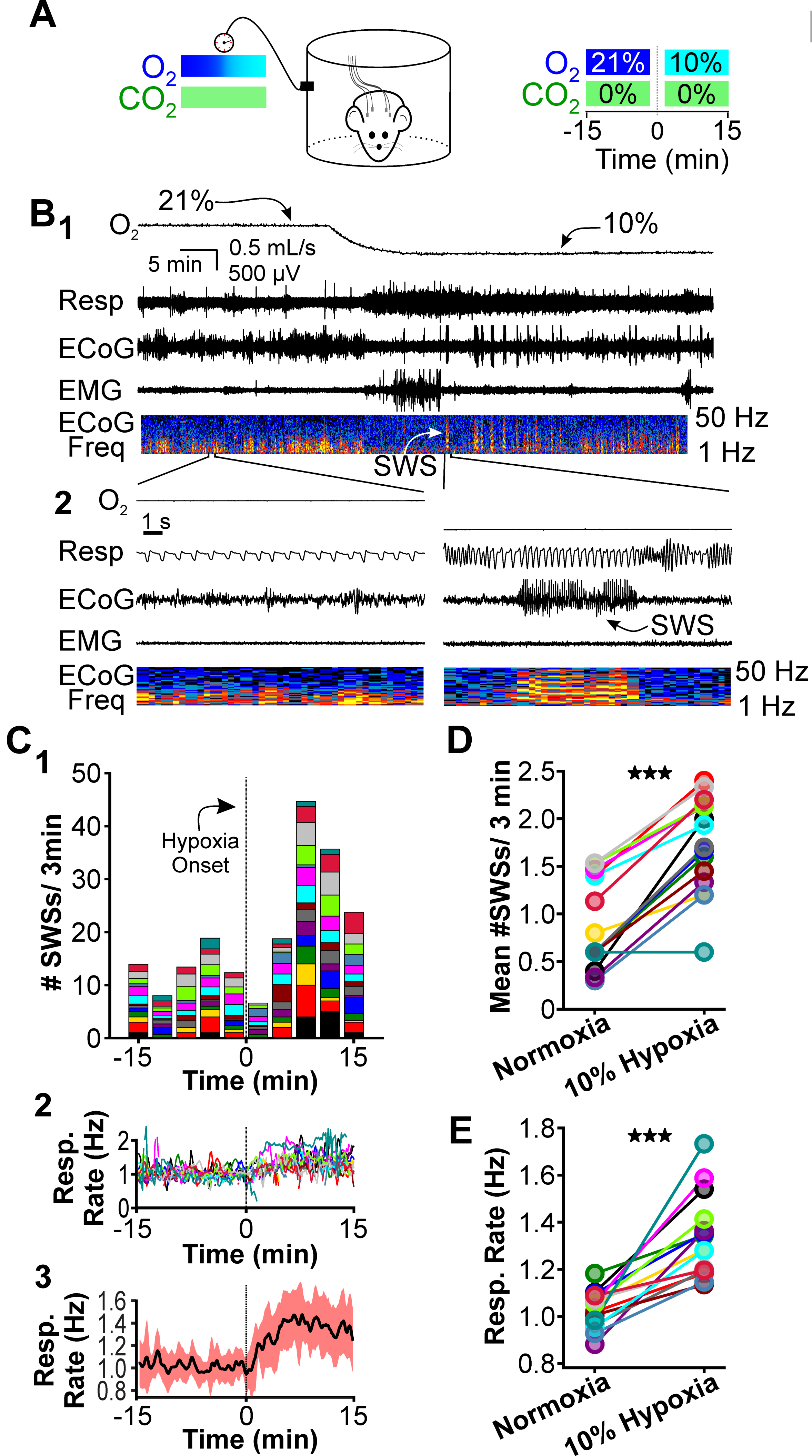
Figure 1
A
O2
CO2
O2 21% 10%
CO2 0% 0%
-15 0 15
Time (min)
B1
21%
O2
10%
5 min
0.5 mL/s
500 µV
Resp
ECoG
EMG
ECoG Freq
50 Hz
1 Hz
SWS
2
O2
1 s
Resp
ECoG
SWS
EMG
ECoG Freq
50 Hz
1 Hz
C1
SWSs/ 3min
Hypoxia Onset
Time (min)
2
Resp. Rate (Hz)
Time (min)
3
Resp. Rate (Hz)
Time (min)
D
Mean #SWSs/ 3 min
***
Normoxia
10% Hypoxia
E
Resp. Rate (Hz)
***
Normoxia
10% Hypoxia

Figure 2

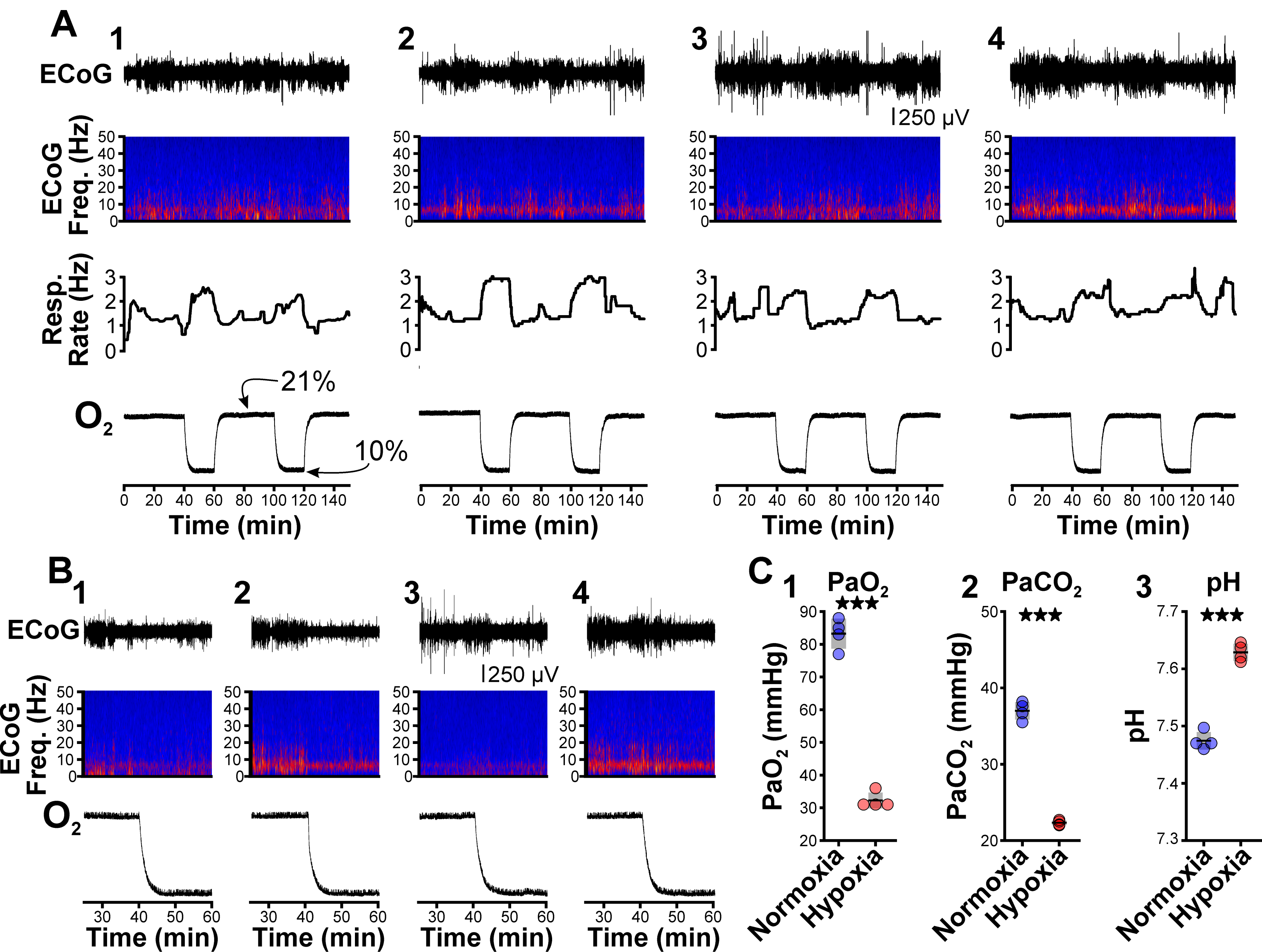

Figure 3

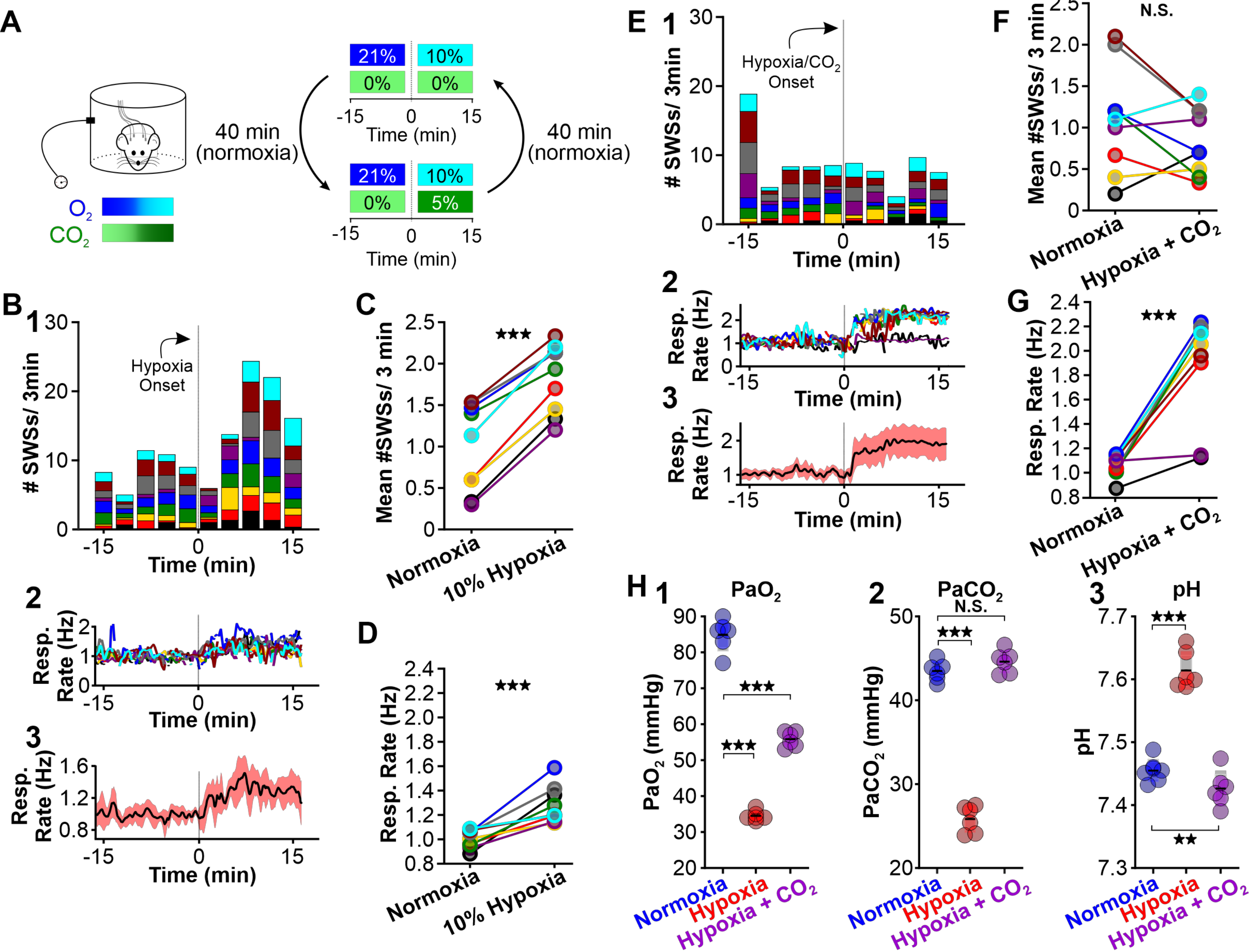

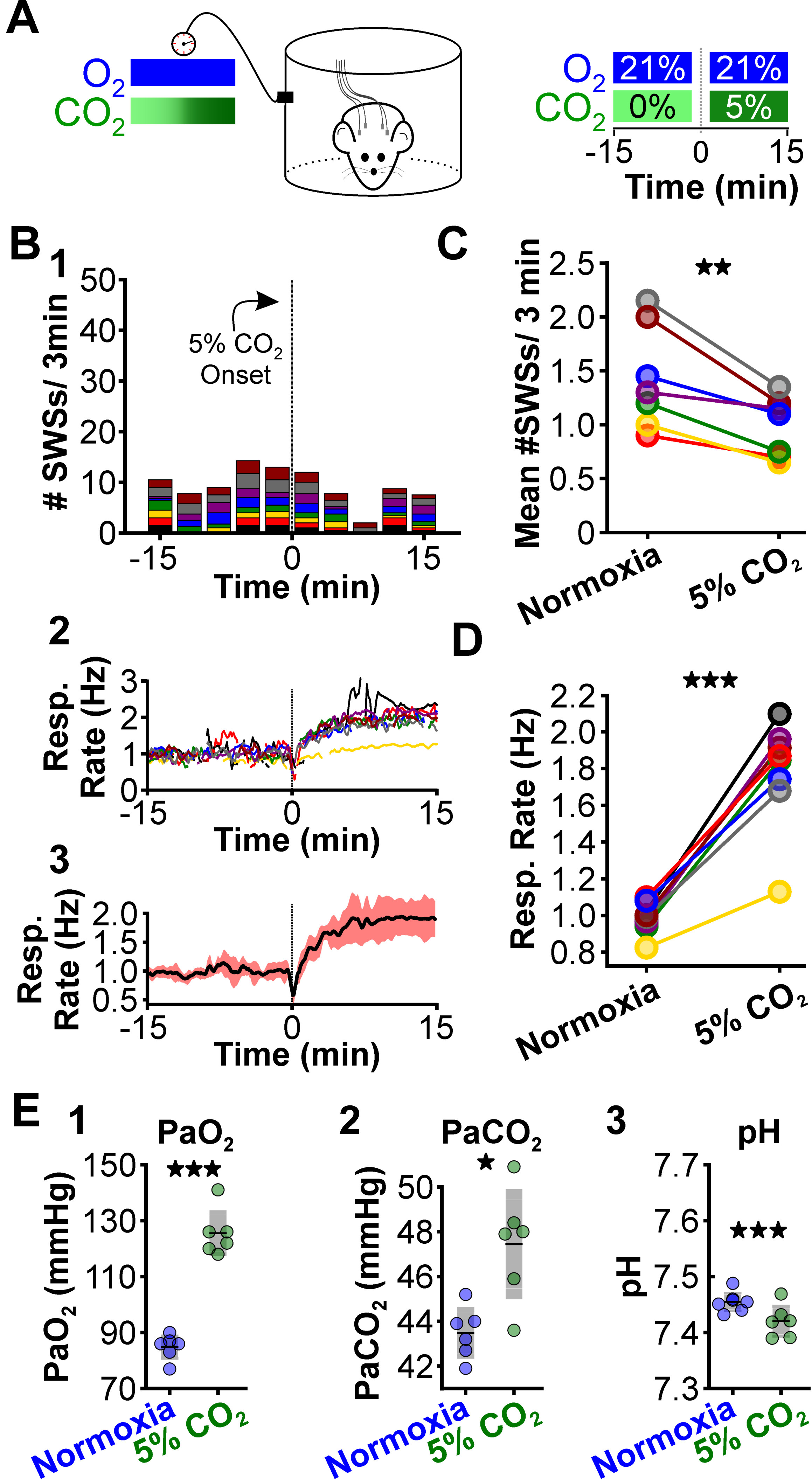
Figure 4
A
O_2
CO_2
O_2 21% 21%
CO_2 0% 5%
-15 0 15
Time (min)
B 1
SWSs/ 3min
5% CO_2 Onset
Time (min)
C
Mean #SWSs/ 3 min
Normoxia
5% CO_2
2
Resp. Rate (Hz)
Time (min)
D
Resp. Rate (Hz)
Normoxia
5% CO_2
3
Resp. Rate (Hz)
Time (min)
E 1
PaO_2
PaO_2 (mmHg)
Normoxia
5% CO_2
2
$PaCO_2$
$PaCO_2$ (mmHg)
Normoxia
5% CO_2
3
pH
pH
Normoxia
5% CO_2

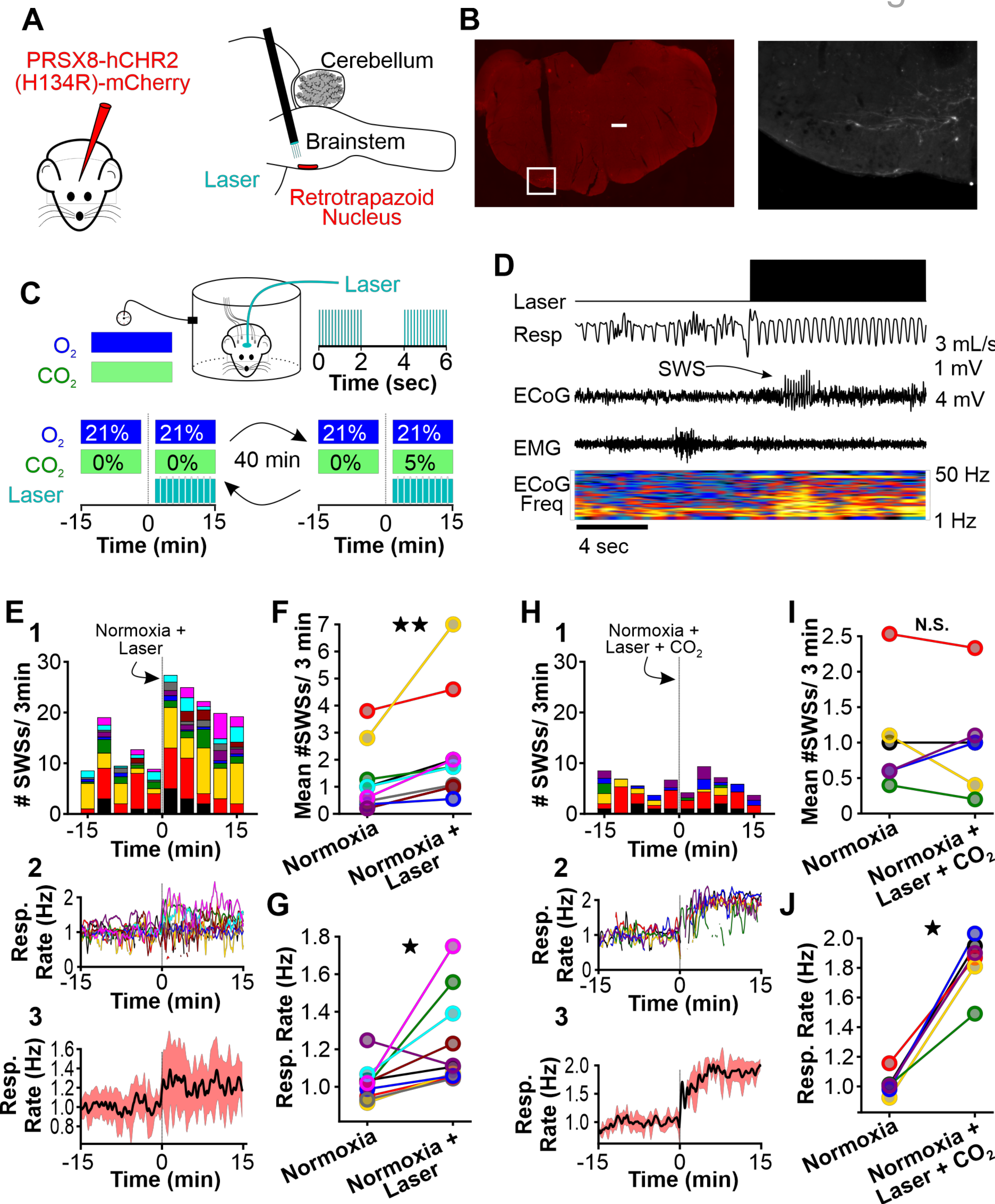

Figure 5
A
PRSX8-hCHR2
(H134R)-mCherry
Cerebellum
Brainstem
Laser
Retrotrapazoid
Nucleus
B
C
Laser
O_2
CO_2
0 2 4 6
Time (sec)
21% 21% 21% 21%
0% 0% 0% 5%
40 min
Laser
-15 0 15
Time (min)
D
Laser
Resp
3 mL/s
SWS
1 mV
ECoG
4 mV
EMG
ECoG Freq
50 Hz
1 Hz
4 sec
E
1
Normoxia + Laser
SWSs/ 3min
Time (min)
2
Resp. Rate (Hz)
3
F
Mean #SWSs/ 3 min
Normoxia
Normoxia + Laser
G
Resp. Rate (Hz)
H
Normoxia + Laser + CO_2
I
N.S.
Normoxia + Laser + CO_2
J

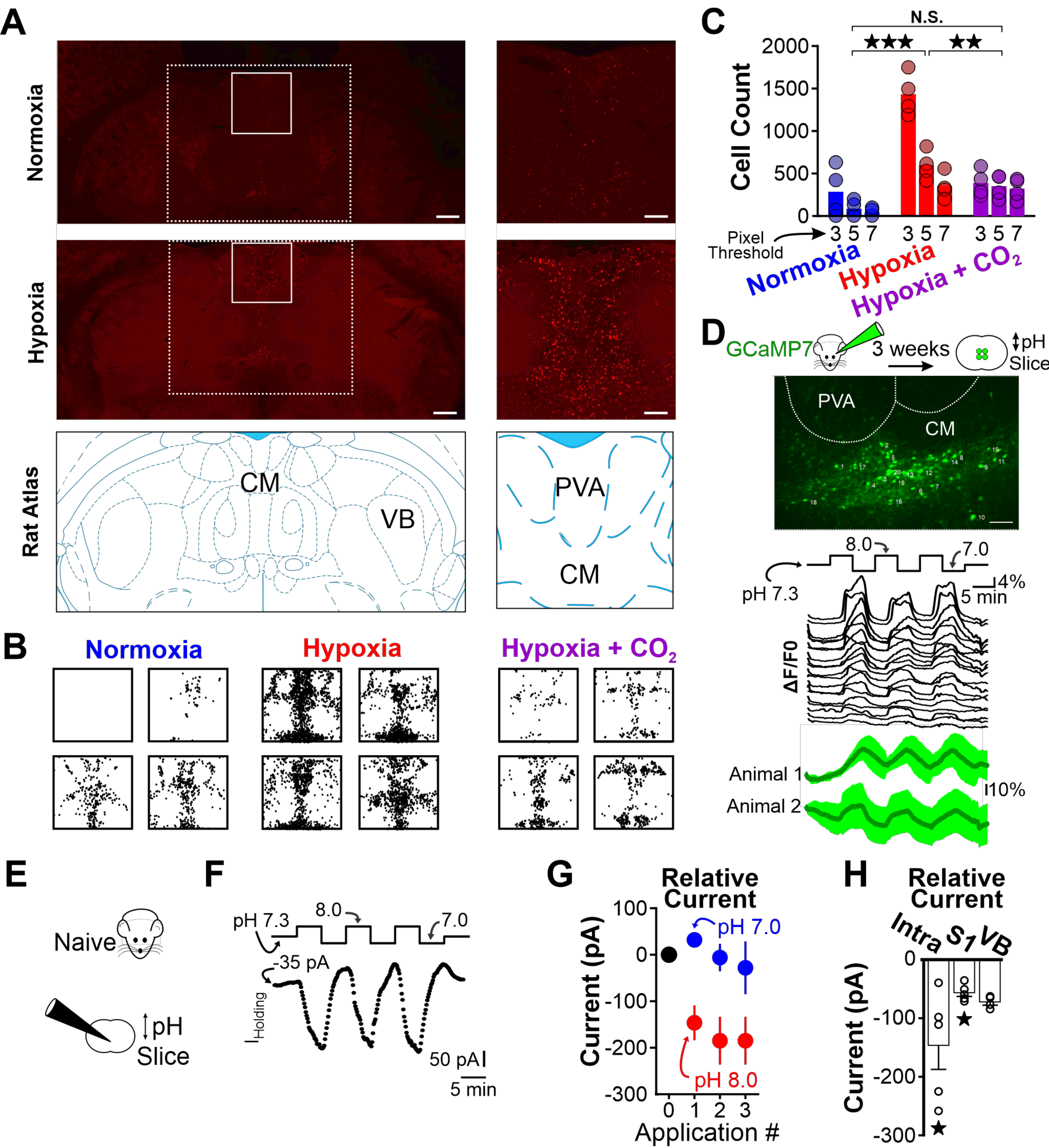
A
Normoxia
Hypoxia
Rat Atlas
CM
VB
PVA
CM
B
Normoxia
Hypoxia
Hypoxia + CO_2
C
N.S.
Cell Count
2000
1500
1000
500
0
Pixel Threshold
3 5 7
Normoxia
Hypoxia
Hypoxia + CO_2
D
GCaMP7
3 weeks
pH
Slice
PVA
CM
8.0
7.0
pH 7.3
4%
5 min
ΔF/F0
Animal 1
Animal 2
10%
E
Naive
pH
Slice
F
pH 7.3
8.0
7.0
-35 pA
$I_{Holding}$
50 pA
5 min
G
Relative Current
Current (pA)
100
0
-100
-200
-300
pH 7.0
pH 8.0
Application #
0 1 2 3
H
Relative Current
Intra
S1
VB
Current (pA)
0
-100
-200
-300